Baseflow Age Distributions and Depth of Active Groundwater Flow in a Snow-Dominated Mountain Headwater Basin

Rosemary W.H. Carroll[1], Andrew H. Manning[2], Richard Niswonger[3], David Marchetti[4], and Kenneth H. Willlams[5,6]

[1]Desert Research Institute, Reno, NV 89512, USA; [2]United States Geological Survey, Denver, CO; [3]United States Geological Survey, Menlo Park, CA; [4]Western Colorado University, Gunnison, CO; [5]Lawrence Berkeley National Laboratory, Berkeley, CA, USA; [6]Rocky Mountain Biological Laboratory, Gothic, CO 81224, USA

Correspondence to: Rosemary W.H. Carroll (Rosemary.Carroll@dri.edu), Division of Hydrologic Sciences, Desert Research Institute, 2215 Raggio Parkway, Reno, NV 89512

Key Points:

- Gas tracer data in baseflow indicates deeper flow through bedrock is an important source to mountain streams.
- Historic variability in baseflow age (3-12 y) is from interflow with groundwater contributions stable (11.8±0.7 y).
- Precipitation defines groundwater age sensitivity, with flow paths getting deeper and older in a slightly drier future.

Abstract. Deeper flows through bedrock in mountain watersheds could be important but lack of data to characterize bedrock properties and link flow paths to snow-dynamics limits understanding. To address data scarcity, we combine a previously published integrated hydrologic model of a snow-dominated, headwater basin with a new method for dating baseflow age using dissolved gas tracers SF_6, N_2, Ar. The original flow model produces shallow groundwater flow (median depth 6 m), very young stream water and is unable to reproduce observed SF_6 concentrations. To match the observed gas data, bedrock permeability is increased to allow a larger fraction of deeper groundwater flow (median depth 110 m). Results indicate that interannual variability in baseflow age (3-12 y) is dictated by the volume of seasonal interflow. Deeper groundwater flow remains stable (11.7±0.7 y) as a function of the ratio of recharge to bedrock hydraulic conductivity (R/K), where recharge is dictated by long-term climate and land use. With sensitivity experiments, we show that information gleaned from gas tracer data to increase bedrock hydraulic conductivity effectively moves this alpine basin away from shallow, topographically controlled groundwater flow with baseflow age relatively insensitive to water inputs (high R/K), and closer toward recharge-controlled conditions, in which a small shift toward a drier future with less snow accumulation will alter the groundwater flow system and increase baseflow age (low R/K). Work stresses the need to explore alternative methods characterizing bedrock properties in mountain basins to better quantify deeper groundwater flow and predict their hydrologic response to change.

Plain Language Summary. Snow in mountain systems is an important water source but little is understood how snow processes dictate groundwater flow paths, the age of water and its sensitivity to climatic or land use change. We use a recently developed stream water gas-tracer experiment in a steep mountain stream in a Colorado River headwater basin. A hydrologic model cannot match gas tracer data if groundwater flow is shallow, moving through the unconsolidated material near land surface, because groundwater moves too quickly. Instead, groundwater must follow deeper flow paths through the fractured granitic bedrock. A sensitivity analysis shows this snow-dominated headwater basin is functioning near a precipitation threshold. With wetter conditions, little change occurs to groundwater flow paths and stream ages are insensitive to changes in climate or forest removal. With small decreases in snowpack accumulation,

groundwater flow paths become increasingly deeper and older. Collecting stream water gas data helped to identify groundwater sensitivity in this basin and to better understand its vulnerability to change.

Keywords: stream water age, mountains; gas tracers; baseflow; hydrologic model; particle tracking

1 Introduction

Baseflow represents stream water derived from both shallow and deep subsurface flow paths that sustain stream discharge late in the season after precipitation or snowmelt events cease. Baseflow is recognized as an important source to stream water in mountainous watersheds (Gabrielli *et al.*, 2012; Rumsey *et al.*, 2015; Hale and McDonnell, 2016; Miller *et al.*, 2016) and reflects the integrated effects of surface processes controlling soil moisture and interflow, groundwater recharge, the subsurface distribution of hydraulic conductivity, and the relative importance of groundwater circulating to different depths. *Interflow*, or shallow flow through the soil zone is typically ephemeral through either strong permeability contrasts or a seasonally rising water table. Interflow reaching a stream network does so on the order of days to weeks. Likewise, the release of bank storage during hydrograph recession moves water from the shallow subsurface into the stream relatively quickly. In contrast, saturated *groundwater* moving through alluvial and bedrock units can have a wide range of flow paths and travel times reflective of lithology, fracture networks and geologic structure (Heidbüchel *et al.*, 2012). The time water spends in the subsurface interacting with host material directly influences biogeochemical processes that control mineral weathering (Winnick *et al.*, 2017), carbon dynamics (Brooks *et al.*, 2015; Perdrial *et al.*, 2018), and the biologic integrety of the river network (Meyer *et al.*, 2007; Missik *et al.*, 2019). Subsurface residence time also indicates the degree of catchment memory of past inputs to reflect hydrologic sensitivity to land use and climate change (McGuire *et al.*, 2005), and potential persistence of contamination (Mahlknecht *et al.*, 2017).

There is a growing recognition that deeper parts of bedrock aquifers in mountain watersheds could be an important component of the watershed hydrologic system, transmitting and storing a larger amount of water and having a larger influence on stream biogeochemical

processes than previously appreciated. Extending the depth of hydrologically active groundwater flow below the soil and saprolite zone to include groundwater movement through deeper, unweathered bedrock are being discussed by (Condon *et al.*, 2020), as are exploring the controls on deeper groundwater flow paths (Markovich *et al.*, 2019). However, the manner in which climate, topography, vegetation, and geology in mountain watersheds affect subsurface flow and resultant stream water age distributions remain poorly understood due to a lack of data characterizing watershed-scale heterogeneity of snow distribution and melt dynamics (Deems et al., 2006; Harpold et al., 2012), soil water and losses to evapotranspiration (Wang and Dickinson, 2012; Allen *et al.*, 2013), subsurface hydraulic properties (Meixner *et al.*, 2016), and active circulation depths (Frisbee et al., 2016).

Lumped parameter approaches have been applied to numerous catchments lacking detailed hydrologic characterization (McGuire and McDonnell, 2006). The age of streamflow (or catchment transit time) is estimated by the convolution of time-varying inputs of an environmental tracer (e.g.,^{3}H, δ^{2}H, δ^{18}O, Cl) applied uniformly across a watershed and lagged through the subsurface by assuming a travel time distribution (e.g. piston-flow, exponential, gamma, Weibull, dispersion) that is adjusted to match observed tracer concentrations in streamflow. Recently, lumped-parameter approaches have been developed that include time variance in travel time distributions to address seasonal changes in flow pathways and mobilization of stored water of varying age (Botter *et al.*, 2011; van der Velde *et al.*, 2012; Harman, 2015). These analytical solutions have been applied to a variety of scenarios, including the influence of snow processes on streamflow (Fang *et al.*, 2019) and selective vegetation uptake (Smith *et al.*, 2018). In contrast to these low-order modeling strategies, numerical mechanistic models and particle tracking can include complex boundary conditions and directly represent physical and hydrological characteristics dictating catchment flow pathways that determine the travel time distribution (Engdahl *et al*., 2016; Maxwell *et al.*, 2016; Danesh-Yazdi *et al.*, 2018). These models provide a powerful platform to study basin sensitivity to changing climate and other conditions, but their application in steep, mountainous basins is still limited by data scarcity; with bedrock hydrologic data on permeability, porosity and flow rates extremely rare, and complicated by the difficulty in characterizing fractured bedrock (Cesano *et al.*, 2003) that are typically dominant in mountain basins. Lack of subsurface data in mountain systems makes quantifying groundwater flow at depth and its relative importance in mountain hydrology

highly uncertain. This knowledge gap remains a major impediment to properly incorporating the deeper subsurface flow system into our hydrologic models and assessing its relative importance to limit our ability to predict how surface water quantity and quality might change under changing climate or land conditions.

To address data scarcity inherent to mountain systems, we apply a method for dating baseflow presented by Sanford et al. (2015) in which stream water N_2, Ar, SF_6 and CFC-113 observations are collected over a 12-hour period. The method's effectiveness has been demonstrated in low-to-moderate-gradient streams, but has not been applied in high-gradient alpine systems where it could be hampered by higher gas exchange velocities (Solomon *et al.* 1998, Gleeson et al., 2018). We combine these gas tracer data with a previously published hydrologic model of a snow-dominated, alpine headwater basin of the Colorado River (Carroll *et al.*, 2019). While simulated hydrology matches observed stream discharge, no directly observed water table elevations or site-specific hydraulic properties of bedrock are available to constrain where and to what depth hydrologically active groundwater flows. Our combined gas tracer and numerical modeling approach builds on previous work (Kolbe *et al.*, 2016; Ameli *et al.*, 2018) by increasing scale of analysis and adding snow dynamics in space and time to explore the (i) relative importance of shallow versus deeper groundwater flow contributions to stream water in a mountainous watershed as a function of baseflow age, (ii) principal controls on groundwater flow pathways, and (iii) sensitivity of groundwater flow pathways to climate and land use.

2 Site Description

The upper East River is a seasonally snow covered, mountainous watershed in the headwaters of the Upper Colorado River (Figure 1) located near Crested Butte, Colorado. A comprehensive overview of the site is provided by others (Carroll *et al.*, 2018; Hubbard *et al.*, 2018). In brief, climate is continental subarctic and stream discharge is dominated by snowmelt with peak flows occurring in early June and receding through the summer and fall. Monsoon rains occur in the summer months and can cause small transient increases in stream flow. The watershed is approximately 85 km^2, and contains pristine alpine, subalpine, montane and riparian ecosystems. This study is focused on Copper Creek (24 km^2), the largest tributary of the upper East River. Land cover is predominantly barren alpine (50%) and conifer forests (36%) with

smaller representations of meadows, shrubs, and aspen. Elevations range from 2880 m to 4128 m. The upper portion of the watershed and adjacent peaks are underlain by Tertiary granodiorite. This younger, intrusive rock has upturned Paleozoic and Mesozoic sedimentary strata into steeply dipping hydrostratigraphic units that underlay the lower portion of Copper Creek (Figure 1b). Talus, rock glaciers and alluvial fans dominate surficial deposits within Copper Creek's glacially sculpted valleys (Gaskill et al., 1991). Descriptions of individual geologic units are provided in Table 1.

Hydrologic modeling of Copper Creek (Carroll *et al.*, 2019) estimates average annual precipitation in Copper Creek is 1.39±0.27 m/y of which 69±9% is snow. Annually, the basin is energy limited (potential ET < precipitation) with average ET losses equal to 36% of annual precipitation. The bulk of ET is lost from the soil zone (67% ET) and lesser amounts are lost from sublimation (13% ET), canopy evaporation (9% ET) and groundwater ET (11% ET). On average, stream water is 65% interflow and 35% groundwater, with interflow contributions declining non-linearly with increased aridity due to increased proportional losses to ET. Groundwater volumetric contributions to streamflow remain relatively stable across the historic period, with the model estimating more than 60% of groundwater moving through the alluvium overlaying less permeable bedrock.

3. Methods

3.1 Atmospheric Gas Tracers

3.1.1. Sample Collection and Analysis

Stream water dissolved gas sample were collected following the general approach of Sanford et al. (2015) in which samples are collected hourly for two relatively inert atmospheric gases (N_2 and Ar) and two gas age-tracers (SF_6 and CFC-113) over a 12 h period. The stream sampling site, CC03 (Figure 1), was chosen because it is located low the watershed, allowing an integrated baseflow age estimate representing most of the watershed, but is above a steep canyon containing large waterfalls. The stream section immediately upstream of the site was free of deep pools and zones of anomalously high turbulence. The location is 2 km above the confluence of Copper Creek to the East River and resides just below the geologic interface between the upper basin bedrock containing granodiorite and the lower basin containing sedimentary strata of

higher permeability. The experiment was conducted on August 27, 2017, which is late enough in the year to avoid monsoon rains and possible surface runoff contributions to the stream, yet early enough to still have large diurnal stream temperature fluctuations characteristic of summer months. Stream water temperature was measured every 5 minutes (Solinst Level Logger Edge M3001 LT F6/M2) beginning the day before and extending through the gas sampling period. Local barometric pressure was obtained from a Rocky Mountain Biological Laboratory weather station located 1.9 km from CC03 (Figure 1) and adjusted for the elevational difference of 70 m. Water samples for N_2, Ar, SF_6, and CFCs were collected in duplicate every hour from 8:30 am to 8:30 pm (Supporting Information, Tables S1 and S2), to capture minimum and maximum diurnal stream fluctuation. Samples were collected using a peristaltic pump and polyethylene tubing placed several centimetres off the stream bed. Sample containers were filled using techniques described at the United States Geological Survey's Reston Groundwater Dating Laboratory (USGS Dating Lab) website (USGS, 2017), stored on ice, and shipped the next day to the USGS Dating Lab for analysis. Samples for CFCs and SF_6 were analysed using purge and trap gas chromatography with an electron capture detector (GC-ECD) (Busenberg & Plummer 1992, 2002), while samples for N_2 and Ar were analysed using gas chromatography with a thermal conductivity detector (GC-TCD, USGS 2017). Measurement errors based on the sample duplicates are 1.7% for N_2, 1.4% for Ar, and 1% for SF_6 and CFC-113, these being consistent with lab-reported errors (USGS, 2017).

Dissolved SF_6 concentrations were measured in three perennial springs located in the vicinity of CC03 to provide independent groundwater age information (Figure 1). Samples were collected in July and October 2017. Argon and N_2 were also measured in two of these springs. Spring CCS is located higher in the Copper Creek watershed 1.7 km from CC03, and springs RCS and RGS are located within adjacent tributaries of the East River 5.4 km and 6.7 km from CC03, respectively. All three springs are at elevations between 3200 to 3500 m. Dissolved gases were collected using a peristaltic pump with the intake attached to a PushPoint pore water sampler (PPX36, https://www.mheproducts.com/) inserted into the shallow sediment at the bottom of each spring pool. Sample collection followed the same protocols indicated above (USGS 2017) and all samples were analysed by the USGS Dating Lab.

3.1.2. Tracer Data Interpretation

In the technique developed by Sanford et al. (2015), measured stream dissolved gas concentrations are used with stream temperature and local atmospheric pressure measurements to simultaneously solve for the rates of gas and water exchange into and out of the stream, as well as the concentration of the gases in groundwater discharging into the stream. A control volume approach accounts for all inputs and outputs of water and gas along the length of the stream and assumes gases are non-reactive. The change in gas concentration in the stream (C_s [M/L^3]) with time [t] is described by the following mass balance equation (equation 11 in Sanford et al. 2015):

$$\frac{dC_s}{dt} = \frac{1}{\tau_w}\left(C_{gw} - C_s\right) - \frac{1}{\tau_g}(C_s - C_e), \quad (1)$$

where C_{gw} [M/L^3] is the gas concentration in groundwater discharging into the stream; C_e, [M/L^3] is the atmospheric equilibrium gas concentration; τ_w [t] is the water residence time in the stream, equal to the stream depth divided by the rate of upward groundwater seepage through the streambed; and τ_g [t] is the gas residence time in the stream, equal to the stream water depth divided by the gas-transfer velocity (v_g [L/t]). The gas-transfer velocity governs the rate of gas exchange between the stream and the atmosphere. Stream concentrations will be an intermediate value between C_{gw} and C_e; if $\tau_w << \tau_g$ then C_s approaches C_{gw} and if $\tau_w >> \tau_g$ then C_s approaches C_e and it is difficult to discern C_{gw}.

The equilibrium gas concentration fluctuates due to diurnal stream temperature oscillations, and can be computed using Henry's Law with the form:

$$C_e = P_a e^{a+b\left(\frac{100}{T}\right)+c\ln\left(\frac{T}{100}\right)+d\left(\frac{T}{100}\right)}, \quad (2)$$

where: P_a is the dry atmospheric pressure [atm]; T is the stream temperature [Kelvin]; and *a*, *b*, *c* and *d* are gas-specific coefficients. The method takes advantage of the oscillatory variation of C_e with time to simultaneously solve for C_{gw}, τ_w, and τ_g for each gas using an explicit finite difference representation of equation (1). Because τ_g is one of the computed parameters, a key advantage of this method, over many other techniques using dissolved gas tracers in streams to characterize groundwater inputs, is that it does not require an independent determination of v_g. The purpose of measuring concentrations of N_2 and Ar in addition to the age tracer gases is that

they can estimate the recharge temperature (T_r) and excess air concentration (A_e, [M/L^3]) for groundwater. The recharge temperature is the temperature at the water table at the recharge location, and A_e is an excess component of air dissolved in groundwater due to the dissolution of air bubbles trapped when the water table rises during recharge events (Stute and Schlosser, 2000). The unfractionated-air model of excess air formation (Aeschbach-Hertig *et al.*, 2000) is assumed in this study. When T_r and A_e are known, estimated values of C_{gw} for SF_6 and CFC-113 are used to calculate their atmospheric concentrations at the time of recharge, which in turn provides a mean age for baseflow through use of an assumed form of a travel time distribution (Busenberg and Plummer, 2002). Sanford et al. (2015) assumes a Weibull distribution in which the cumulative distribution function (F) over time is defined as,

$$F(t) = 1 - e^{-(kt)^n}, \quad (3)$$

in which the scale parameter (k) and shape parameter (n) are adjusted to match the computed atmospheric concentration to the historical record (USGS 2017). The Weibull distribution is equivalent to the exponential mixing model when $n = 1$.

Values of C_{gw} for each gas are estimated using a modified version of the Excel spreadsheet calculator developed by Sanford et al. (2015), which minimizes the misfit between measured and modeled values of C_s employing the automated General Reduced Gradient solver tool (provided as supporting documentation). Modifications include a reduced time step from 0.25 h to 0.1 h and expressing the misfit between measured and modeled values with the sum chi-squared (χ^2), rather the sum squared error, to assess statistical significance of predicted water column concentrations. The sum χ^2 is the square of the difference in measured and modeled values divided by the square of the measurement error. Following Sanford et al. (2015), up to nine parameters can be adjusted to match stream gas concentrations: T_r, A_e, groundwater excess N_2 (potentially present from denitrification), τ_w, a single gas residence time for N_2 and Ar, gas residence times for SF_6 and CFC-113, and C_{gw} values for SF_6 and CFC-113.

For springs CCS and RCS, T_r and A_e values were derived from measured N_2 and Ar concentrations and used to compute a piston-flow groundwater age (assumes a uniform age for all sampled water) from the measured SF_6 concentration using standard methods (USGS 2017). The recharge elevation was assumed to be the approximate mean elevation of the portion of the

263 watershed directly upslope of the sampled spring. For spring RGS, Ar and N_2 were not collected
264 and the mean T_r and A_e from the other two springs was used in the calculation of the piston-flow
265 age.

266 **3.2 Integrated Hydrologic Model**

267 Carroll et al., (2019) simulated energy and water budget components in Copper Creek
268 using the USGS Groundwater and Surface water Flow model (GSFLOW, Markstrom et al.,
269 2008). GSFLOW dynamically couples the USGS Precipitation-Runoff Modeling System
270 (PRMS, Markstrom et al., 2015) and the Newton formulation of the USGS 3D Modular
271 Groundwater Flow model (Harbaugh, 2005; Niswonger et al., 2011). The model describes daily
272 surface and groundwater interactions related to evapotranspiration (ET) including soil
273 evaporation and plant transpiration, canopy interception, snow sublimation and groundwater ET.
274 The hydrologic model also estimates interflow, groundwater recharge, change in groundwater
275 storage, as well as groundwater-surface water exchanges derived from differential gradients
276 between groundwater and stream water elevations (Huntington and Niswonger, 2012), and
277 deeper groundwater flow based on lithology and geologic structure.

278 The finite difference grid resolution is 100-m with elevations resampled from the USGS
279 National Elevation Dataset. Landfire (2015) was used to derive parameters of dominant cover
280 type (Figure S5b), summer and winter cover density, canopy interception characteristics for
281 snow and rain, and transmission coefficients for shortwave solar radiation. Climate for water
282 years (October 1-September 30) 1987 to 2018 were simulated using two proximal Snow
283 Telemetry (SNOTEL) stations (Figure 1) and LiDAR derived snow water equivalent from the
284 Airborne Snow Observatory (Painter *et al.*, 2016) (Figure S5a). The largest snow accumulation
285 occurs in high elevation cirques, upper subalpine and north-eastern aspects of the basin. LiDAR
286 snow observations implicitly account for snow redistribution by wind and avalanche and provide
287 confidence on the location and timing of water inputs to the basin. Maximum soil water storage
288 is conceptualized as a field capacity threshold above which water is partitioned to either lateral
289 interflow or allowed to percolate downward via gravity drainage into the unsaturated zone
290 (recharge). The spatial distribution of soil storage is the product of rooting depth obtained from
291 Landfire (2015) and available water content as a function of soil type (NRCS, 1991). The Copper
292 Creek geologic model (Figure S5c) contains nine hydrostratigraphic units with 12 layers ranging

in thickness from 8 to 120 m for a total thickness of 400 m. Transient water table gradients (e.g. Oct 1, 2016 provided in Figured S5d) dictate alluvial and bedrock water sources to the stream. Water table elevations are shallow and steep in the low permeable granodiorite in the upper portions of the watershed. Fracture networks are not simulated. Instead, we use effective hydraulic conductivity that decreases with depth , with surface hydraulic conductivity optimized to match average observed baseflow at the stream gauge located at the terminus of the basin.

3.2.1 Simulated Baseflow Age Distribution

Baseflow is simulated as the sum of (i) saturated groundwater flow through alluvial and bedrock units, and (ii) seasonal, shallow interflow. These two components are handled separately and combined into a single baseflow age distribution representative of late summer stream water. First, the age of saturated groundwater flow paths are estimated using a particle tracking algorithm in which particles are draped on the water table surface and allowed to move through the watershed as a function of groundwater boundary fluxes and associated water table gradients (Mpath7, Pollock, 2016). Individual flow path ages are weighted by recharge: defined as water seepage below the soil zone plus ephemeral stream leakage to groundwater and corrected for volume weighted age of water lost back to the atmosphere via groundwater ET. Second, the contributing volume of interflow in the river during the late August is assumed less than one year old and added to groundwater age distribution calculated with particle tracking.

Both transient and steady state particle tracking simulations use a similar methodology. Transient simulations evaluate the efficacy of the hydrologic model to generate a baseflow age distribution able to reproduce the observed gas tracer water column concentrations at the end of August 2017. Initial water table elevations and water fluxes for water year 2017 initiate the transient particle tracking simulation and then historical water fluxes for water years 1987 to 2018 are repeated until all particles exit the watershed. A Weibull distribution (*k* and *n*, equation 3) is adjusted to the flow model baseflow age distribution to solve for stream water SF_6 water column concentrations. The calculation of SF_6 water column concentrations uses tracer-based estimates of A_e and T_r, an assumed recharge elevation of 3400 m (the approximate mean elevation of the watershed above CC03), and the historical atmospheric concentration record (USGS 2017). If the age distribution is unable to replicate observed stream concentrations based on the sum χ^2, then subsurface porosity is adjusted. If adjusting porosity is insufficient to create a

statistically significant reproduction of observed gas tracers, then the original calibration of bedrock hydraulic properties in the flow model presented by (Carroll *et al.*, 2019) are revisited based on groundwater age distribution sensitivity to geologic parameterization (refer to Supporting Information S.2). Using the final model, additional transient simulations are initiated to explore interannual variability across a range in historical water years. These years include an extremely wet year (1995), a dry year at the end of a multi-year drought (2002), a dry year with a strong monsoon (2012), a dry year with a weak monsoon (2018) and the median water year (1998).

Steady state particle tracking simulations provide information on how deeper groundwater flow paths may change by shifting the historical mean groundwater condition as a function of altering precipitation, temperature or forest presence. The historical median water year (1998) is used as a baseline condition from which precipitation is incrementally adjusted by 0.4 to 1.8 the historic daily value with no warming (+0°C). This is repeated for +4°C and +10°C warming applied to both minimum and maximum daily temperatures. The +4°C condition falls in the range of expected end-of-century temperature increase in the East River (Hay *et al.*, 2011) while +10°C forces all snow to fall as rain. The effect of spatial distribution of precipitation and temperature across the watershed is also tested by assigning spatially uniform daily values based on average historic median water year daily inputs. This removes gradients associated with elevation, storm tracking and snow redistribution. Lastly, the relative importance of forest influences on energy and water budget partitioning and baseflow age are explored by removing deciduous and conifer forests from the basin. Forests were replaced by a barren cover type and recharacterization of transmission coefficients for shortwave radiation, interception of precipitation and rooting depths. Soil storage and its conductance were not altered. For each hypothetical scenario, GSFLOW daily stress is simulated over a complete water year and repeated until quasi-steady state conditions occur. Quasi-steady state is complete when combined changes in saturated and unsaturated groundwater storage were less than 1% the annual water budget. Cell specific groundwater fluxes (recharge, ephemeral stream losses and groundwater ET) are aggregated to an annual sum for each model cell and applied to the steady state groundwater model for particle tracking.

. 4 Results

4.1 Atmospheric Gas Tracers

Measured N_2, Ar and SF_6 concentrations along with computed T_r, A_e, and piston-flow age values for the three sampled springs are shown in Tables S3 and S4. Computed SF_6 piston-flow ages range from 3 y to 14 y. The samples from CCS were collected in June after a large snowpack accumulation and had the youngest ages (3 to 6 y). The younger ages and warm mean T_r of 9.2°C (near the top of the expected range of 0-10°C; see Supporting Information S.1) suggests that CCS either contained a substantial fraction of very young water recharged only weeks prior to sampling during the spring, or the sampled water partially re-equilibrated with the atmosphere. The other springs were sampled in October with piston-flow ages 7 to 14. Mean T_r and A_e values for the spring samples are 5.5°C and 0.0011 cm^3STP/g, respectively.

Measured concentrations of N_2 and Ar in Copper Creek are very close to computed equilibrium concentrations for the stream water (Table S2, Figure S2a,b), indicating a relatively small τ_g (relatively large v_g) for N_2 and Ar. Because v_g is generally positively correlated with stream gradient (Gleeson *et al.*, 2018), a relatively large v_g is consistent with Copper Creek's steep gradient of ~0.09 above the sample location. In contrast, measured concentrations of SF_6 and CFC-113 are below equilibrium concentrations for the stream water (Table S2, Figure S2c,d). This suggests that: (a) the age of groundwater discharging into the stream is sufficiently large that the difference between C_{gw} and C_e is non-trivial (on the order of years rather than weeks/months); and (b) though τ_g values are relatively small for Copper Creek, they are still large enough so that the age-tracer C_{gw} signal is maintained in the stream. Therefore, despite Copper Creek's high gradient, v_g for the age-tracer gases were sufficiently slow to permit application of the method proposed by Sanford et al. (2015). Although SF_6 and CFC-113 are generally well mixed in the atmosphere, local atmospheric concentrations on the day of sampling could be slightly below the northern hemisphere 6-month average values used to compute C_e (USGS, 2017), such that C_s is actually equal to C_e to invalidate the method. A comparison of the atmospheric concentrations required to produce the observed stream concentrations with multiple North American atmospheric monitoring sites indicates that this scenario was unlikely (Figure S1).

The measured gas concentrations in the stream do not provide a unique solution for C_{gw} for either SF_6 or CFC-113, allowing a broad range of possible ages for baseflow (Supporting Information S.1). However, the range of allowable age-tracer C_{gw} values is well-constrained on the high end because atmospheric concentrations of these age tracers have generally increased since their introduction in the mid-20th century. This high-end constraint on C_{gw} can potentially provide a reliable minimum age constraint for baseflow. Note that allowable CFC-113 C_{gw} values are sufficiently low to indicate recharge predominantly before the mid-1990's when atmospheric concentrations started decreasing. The CFC-113 concentrations are discarded from the analysis because, for a given value of τ_w, the estimated CFC-113 C_{gw} consistently produced a substantially older mean age (generally by >10 y) than produced by the simultaneously estimated SF_6 C_{gw} regardless of the assumed form of the travel time distribution. This age discrepancy is likely due to either SF_6 contamination from terrigenic production in the subsurface (e.g. Friedrich et al. 2013), CFC-113 degradation occurring under low-oxygen conditions in parts of the aquifer (e.g. Bockgard et al. 2004) or both. A similar discrepancy was observed by Sanford et al. (2015) at some sites in northern Virginia, USA, and they attributed this to terrigenic SF_6 contributions based on evidence of terrigenic SF_6 in groundwater samples from local springs and wells in which concentrations reflected impossibly high atmospheric concentrations. For the Copper Creek samples, we believe that CFC-113 degradation is a more likely explanation because the spring samples in the East River display no clear evidence of terrigenic SF_6 contributions. Furthermore, the range of allowable CFC-113 piston-flow and exponential mean ages for baseflow (>30 y) are substantially older than most reported groundwater ages for other mountain watersheds underlain by predominantly crystalline rock (generally <20 y; Plummer et al. 2001; Manning 2009; Visser et al. 2019; Manning et al. 2019). Regardless, using the SF_6 measurements to determine a maximum C_{gw} and minimum baseflow age is a more appropriate and conservative approach because any terrigenic additions would increase the estimated C_{gw} whereas CFC-113 degradation would decrease the estimated C_{gw}.

The maximum SF_6 C_{gw} was estimated through a series of best-fit model solutions in which CFC-113 was excluded from the analysis, a range of SF_6 C_{gw} values were specified, and resulting model fits were evaluated (Table 2, Figure 2a). Model fits, defined by the sum χ^2 metric with a $p > 0.1$, to observed stream water SF_6 concentrations are similar and acceptable for SF_6 C_{gw} values up to about 2.2 fmol/L. For C_{gw} > 2.3 fmol/L, model fits declining rapidly,

becoming unacceptable. For the purposes of numeric modeling, we move forward with the requirement that any flow-model-generated age distribution must produce an SF_6 C_{gw} concentration <2.3 fmol/L to be consistent with the stream age-tracer measurements. As noted above in Section 3.1.2, values of T_r and A_e, must be assumed to compute C_{gw} for a given age distribution. The fact that C_s and C_e are essentially equal for N_2 and Ar means that the stream N_2 and Ar measurements provide no meaningful constraints on these parameters (Figure S3). Therefore, the mean T_r and A_e values derived from the spring samples are assumed in the computation of C_{gw} for the flow-model-generated age distributions (see Supplementary Information S.1 for additional discussion).

4.2 Integrated Hydrologic Model

4.2.1 Baseflow Age Calibration

Simulated streamflow and the fraction of streamflow that is interflow for a range of historically variable water years is provided in Figure 3. Interflow dominates stream water source during snow melt (April-July) and can be bolstered in the summer and fall by monsoon rains. Interflow contributions to Copper Creek in late August 2017 during the gas tracer experiment are 22% and align with the same fraction of shallow, soil derived flow in the median water year (1998) and a dry water year with a good monsoon (2012). Figure 4 shows the resulting baseflow age distribution at the sampling location CC03 using the originally published flow model. Median baseflow age is 1.5 y and water table elevations are shallow (median depth of flow 6 m) with 64% of recharged water moving through the top model layer which is predominantly alluvium. Figure 5a illustrates the hyper-localized, topographically controlled and very young groundwater flow paths above the sampling location where granodiorite is the dominant bedrock. Using a Weibull distribution fit to the GSFLOW baseflow age output (k=0.28, n=0.44), the SF_6 groundwater concentration is calculated at 2.74 fmol/L and the sum χ^2 is 147 indicating a statistically insignificant replication of SF_6 stream concentrations (Figure 2).

Geologic parameter adjustments based on a sensitivity analysis (refer to Supporting Information S.2. Figure S6,7) to promote older baseflow, with the goal of lowering estimated SF_6 groundwater concentrations, included: increasing the granodiorite hydraulic conductivity four-

441 fold over the original value of 1.16×10^{-7} m/s to 4.66×10^{-7} m/s, and lowering the ratio of
442 horizontal to vertical hydraulic conductivity, or VKA from 10 to 3. Accompanying changes in
443 bedrock properties was a slight increase in soil storage to replicate observed stream discharge
444 (Nash Sutcliffe Efficiency Log discharge = 0.78). Bedrock reparameterization lowers predicted
445 water table elevations (median depth of groundwater flow equal to 115 m), reduces groundwater
446 flow through the alluvium from 64% to 22% (Figure 4b), and produces a baseflow age
447 distribution (Weibull k = 0.79, n = 0.66, Figure 4a) capable of reproducing groundwater SF_6
448 concentration of 2.2 fmol/L in order to statistically replicate SF_6 stream water concentrations
449 (sum χ^2 = 12.9, Figure 2). The hydrologic model produces a median age at CC03 of 7.5 y, which
450 falls within the range of October ages for perennial springs to provide added confidence in the
451 approach. Figure 5b shows older flow path are now generated in the upper confines of Copper
452 Creek that are less constrained by topography than the original model.

453 **4.2.3 Baseflow Age Sensitivity**

454 Using the calibrated model to assess a variety of historic water years indicates
455 groundwater age contributions are relatively stable 11.8 ±0.7 y, while late summer baseflow ages
456 range between 3 and 12 years as a function of contributing interflow (Table 3, Figure S8). A
457 sensitivity analysis perturbing long term climate from its median condition by incremental
458 changes in the historic median water year daily precipitation show groundwater age distributions
459 (Figure S9) shift progressively toward older water with decreased precipitation. Warming by
460 +4°C decreases groundwater ages slightly for very wet conditions. Warming during a drought
461 (e.g. 0.8P) removes relatively younger water while warming during a more intensive drought
462 (e.g. 0.4P) affects all flow paths and the entire distribution shifts older. Warming the basin until
463 snow is converted to rain (+10°C) increases groundwater ages for all conditions, but increases
464 are most dramatic under a drier climate. Removing the forest from Copper Creek increases
465 recharge and shifts groundwater toward younger ages with decreased ages most notable during
466 dry conditions. The median ages from all scenarios increase with decreasing precipitation and
467 collapse about a single exponential function defined by average annual net recharge (Figure 6).
468 Assuming spatially uniform climate effectively decreases net recharge for the same amount of
469 annual precipitation. This produces a groundwater age distribution more closely matched to
470 decreasing precipitation by 20% over the historical median condition.

5 Discussion

Stream water source in the late summer is composed of both shallow epemeral flow through soil and saporlite and saturated groudnwater flow through alluvium and bedrock units. Deeper groudnwater flow through unweathered bedrock is often treated as negligable in catchment studies (e.g. Kirchner, 2009). However, there is a growing awareness that deeper bedrock flow may be an important component in mountain hydrology (Gabrielli *et al.*, 2012; Hale and McDonnell, 2016) and a general call to include the bottom of the groundwater system in our conceptual model (Brantley *et al.*, 2007; Brooks *et al.*, 2015). However, a fundemental challeng in hydrology is to define and observe where the bottom of the watershed occurs and to assess if it is important (Condon *et al.*, 2020). The challenge is amplified in steep, snow dominated mountain watersheds. These watersheds provide 60-90% of the freshwater world wide (Viviroli and Weingartner, 2008) and are especially vulnerable to climate change (IPCC, 2019) but data describing bedrock properties and deep subsurface flow is scarse in these systems and uncertainty in predicting how projected warming or reduced snowpack will affect streamflow response as well as redox-sensitive and time-sensitive reactions in respone to changing water tables and travel times remain large (Manning *et al.*, 2013; Meixner *et al.*, 2016).

5.1. Age of Baseflow and Depth of Active Groundwater Flow

To address uncertainty in depth of groundwater flow, we present a novel approach that combines a sophisticated numierical hydrologic model and a new method for dating baseflow using dissolved N_2, Ar and SF_6. The gas tracer experimental approach is relatively conveneinent and cost effective as it takes a single day to perform and does not require expensive drilling. Drilling, which is often impossible due to logistical challenges related to steep topography, deep snowpack and (in our case) Wilderness designation. The stream tracer experiment was not originally designed for steep, turbulent rivers with fast gas exchange velocities to the atmosphere and its use in Copper Creek is, in of itself, a methodological question on its effectiveness in alpine environments. Because of fast gas velocities, the approach could not provide a unique baseflow age determination in Copper Creek. However, it did provide a relatively robust upper limit on the groundwater SF_6 concentration. This maximum concentration is then used to test the

validity of the flow model generated baseflow age distribution, and thereby establish the lower limit on the mean age of this distribution.

The originally published GSFLOW model calibrated to stream discharge over a multi-decadal period, generates shallow groundwater flow moving predominantly through alluvium situated on much less conductive bedrock. For late summer conditions in 2017, when the tracer experiment was conducted, baseflow median age is estimated very young at 1.5 y. However, this results in statistically insignificant replication of observed SF_6 stream water concentrations. Instead, older groundwater (12.2 y), and a resulting baseflow median age of 7.5 y, must be simulated in the hydrologic model to match observed stream water gas tracer data. With deeper groundwater flow, the recalibrated flow model produces a baseflow median consistent with perennial spring samples collected in October 2017 and in the vicinity of the watershed (10.2 ± 3.4 y). Earlier studies on tranist time modeling in mountainous catchments have tended toward younger ages of 1-5 y (see review by McGuire & McDonnell 2006), in which the de-coding of catchment travel time distributions have primarily relied upon stable isotopes. Yet these tracers cannot inform transport times longer than 4 years and their exclusive use will bias age distributions and understanding of how catchments store and transmit water (Stewart *et al.*, 2012). Techniques for establishing longer travel times include use of atmospheric tracers sensitive to older waters (e.g. ^3H, CFC, SF_6) and a growing number of recent studies suggest baseflow mean ages in headwater streams may be older than previously thought (>10 y) (Cartwright *et al.*, 2018; Cartwright *et al.*, 2020). Similarly, $^3H/^3He$ groundwater ages from 17 stream-side piezometers along a 3.5 km reach of Handcart Gulch in the Colorado Front Range were all between 8.9 y and 19.1 y (Manning *et al.*, 2019). The updated Copper Creek hydrologic model follows this trend in acknowledging older groundwater contributions in mountainous waterersheds.

Re-conceptualization of the Copper Creek grounwdater flow system was largely accomplished by increasing the hydraulic conductivity of the dominant bedrock (granodiorite) above the stream sampling location to lower water table elevations and force more groundwater to travel deeper through the subsurface. One can speculate that high relief watersheds like Copper Creek contain older than expected stream flow, perhaps related to greater permeability and porosity to greater depths due to more intense recent uplift and tectonism associated with mountain building (Williams et al., 2015; Jasechko et al., 2016). Final surface pemeability for the granodiorite

($4.6x10^{-7}$ m/s) falls within the typical range of 10^{-8} to 10^{-6} m/s for zones of active flow in fractured crystaline bedrock in mountain settings; (Katsura *et al.*, 2009; Welch and Allen, 2014). The recalibrated model lowers water table depths such that 22% of recharged water moves through the alluvium and produces a median depth of groundwaterflow equal to 110 m, with 30% of recharged water reaching depths greater than 200 m. This is somewhat deeper than the maximum depth of active groundwater circultion in crystaline rocks of 100-200 m based on a limited number of prior studies (Welch and Allen, 2014; Markovich *et al.*, 2019). However, Frisbee et al. (2017) estimated active circulation upwards to 1000 m in the crystalline metamorphic rocks of the Sangre de Cristo Mountains, New Mexico. Active circulation depths are a function of tectonic history, lithology, structure, and climate (weathering), and characteristic active flow depths for different bedrock geologic conditions in mountain settings remains largely unknown (Markovich *et al.*, 2019).

We acknowledge that constraint on subsurface routing is inherently non-unique in groundwater modeling and the use of a single hydraulic conductance value for a given depth for each hydrostratigraphic unit is simplistic and likely over estimates deep flow paths along the highest elevations in Copper Creek in response to low water table elevations. It is also recognized that our model is constrained to younger flows through our use of the minimum age as determined by the gas tracers to define median age produced by the hydrologic model and that older travel times associated with deep flow paths, that are most sensitive to deep porosity, as not known. Fractured rock porosity is highly uncertain, and complicated by diffusive exchange between mobile water in the fractures and imobile water in the matrix. Effective porosity for age estimates is likely in between matrix and fracture porosity. Unpublished data from a 80 m borehole drillcore in a proximal basin to the East River (Redwell Basin) consisting of contact-metamorphosed interbedded shale and sandstone indicates a matrix porosity of 1-10%, centering around 3%, while fractored porosity in unweathered crystaline rocks <1% is common (Tullborg and Larson, 2006). For comparison, modeled effective porosity of the granodiorite in Copper Creek is set equal to 2.5% (depth ≤ 18 m) and 1.25% (depth > 18 m) and deemed appropriate.

5.2 Controls on Baseflow Age

The physical reality of mountainous watersheds is that heterogenities in the system in combination with spatio-variable inputs create highly diverse flow paths through the watershed.

As a result, the age distribution of stream water is not time invariant but responds dynamically as the nature of overland flow and hydrologic connectivity change, and that flow paths and velocities vary with water storage (Botter, Bertuzzo and Rinaldo, 2011; Van Der Velde *et al.*, 2012; Engdahl, McCallum and Massoudieh, 2016). Transient analysis of individual water years spans the full range of historic climate conditions and results in variability in predicted late summer baseflow median age (3-12 y). This variability is largely due to simulated interflow contributions moving through the soil zone as a result of deep and persistent snowpack and/or a strong monsoon season driving younger flows late in the summer. Results agree with other studies showing the mobilization and mixing of younger shallow water stores with older water following wet periods (Hrachowitz *et al.*, 2013; Howcroft *et al.*, 2018). Specifically, Copper Creek baseflow ages align with recent work in Providence Creek, a granodiorite headwater basin in the southern Sierra Nevada mountains of California, with stream ages ranging from 3.3 to 10.3 y, with wetter years releasing younger water, as determined using ranked storage functions constrained by radioactive isotopes (Visser *et al.*, 2019); and are consistent with spring mean ages in Sagehen, California found to vary 3-7 y between sampling events with age variability controlled by the magnitude of the new fraction (<1 y), which generally correlated positively to annual maximum snow water equivalent (Manning *et al.*, 2012).

In contrast, groundwater flow paths and associated ages showed low variance about the mean (11.8 y) deviating by only 0.7 y despite drastically different snow accumulation and stream dynamics for the years assessed. Interannual stability in groundwater flow represents a basin in equilibrium with its historical climate and watershed structure (i.e. topography, land use, geology). Topographic controls have also long been recognized as controlling local, intermediate and regional groundwater flow systems (Toth, 1963; Winter *et al.*, 2001) and been identified as the single most important control on catchment-scale transport (McGuire *et al.*, 2005). However, the influence of precipitation magnitude and type (Carroll *et al.*, 2017), vegetation (Rukundo and Doğan, 2019), bedrock lithology (Onda *et al.*, 2006), and subsurface connectivity (Tetzlaff *et al.*, 2009) are also recognized in influencing hydrologic partitioning dictating recharge and subsequent groundwater flow to streams. Recharge in mountain watersheds preferentially occurs in the upper subalpine (in part) as a function of large and persistent snowpack snow (Musselman *et al.*, 2008; Broxton *et al.*, 2015; Carroll *et al.*, 2018). We show that maintaining historic median daily climate forcing, but uniformly distributing across Copper Creek, reduces recharge and

lowers water table elevations to produce older groundwater. Similarly, Badger *et al*, (2019), using a distributed hydrologic model and remotely sensed estimates of snowpack found more uniform snow distributions melted out 5 weeks earlier and produced up to 9.5% less stream flow than conditions that allowed for spatial variability. Therefore, capturing the spatial distribution of snow dynamics to better represent recharge is also important to quantifying groundwater flow pathways and age of water exported to a stream network.

Three-dimensional numerical models have provided guiding principles on recharge-controlled versus topographically-controlled water tables that in turn drive the length-scale of flow paths and associated ages in mountain systems (Gleeson and Manning, 2008; Markovich *et al.*, 2019). Figure 7 illustrates the conceptual model of flow paths and baseflow age distributions as a function of water table elevational endmembers dictated by the ratio of recharge to hydraulic conductivity (R/K). High R/K produces higher water table elevations and increases the influence of topographically controlled, local flow paths on stream-flow generation. If water table elevations are high enough to support perennial streams, then the system is likely permeability-limited such that increases in recharge has little effect on changing groundwater flow paths and the median age of groundwater is stable. Conversely, watersheds with lower R/K have deeper water table elevations controlled mainly by the recharge rate. Ephemeral streams emerge, flow paths are less constrained by local topography and groundwater flow conditions become increasingly sensitive to changes in recharge.

Our first round of Copper Creek modeling established a very high R/K in the upper confines of the basin to produce a permeability-limited groundwater flow system with shallow water table elevations in which baseflow ages are buffered from possible decreases in recharge. With model re-evaluation, the R/K ratio in Copper Creek is lowered. The water table is still topographically controlled, but the newly calibrated model suggests Copper Creek is actually very close to the recharge-controlled condition, meaning groundwater flow paths will deepen and baseflow age will increase with relatively small reductions in snow accumulation. The larger the deviation from the historical median precipitation toward a drier state, the greater the sensitivity of groundwater age is to either recharge decreases (warming) or increases (forest removal). Ameli et al. (2018), using a combination of tritium tracer and a semi-analytical flow and transport modeling strategy in a New Zealand headwater basin, also found groundwater flow paths lengthen and water ages contributing to streams increase indirectly to recharge rate.

However, this rain-dominated catchment underlain by early Pleistocene conglomerate likely reflects a recharged-controlled basin that was not readily apparent in Copper Creek. Our study emphasizes that assuming a snowmelt-dominated mountain watershed is permeability-limited simply because it is underlain by low-permeable crystalline rock is potentially misguided. Instead, our results suggest that proper characterization of the deeper bedrock groundwater flow system is fundamentally important to establishing R/K and determining how a watershed will respond to changing climate and land use.

6. Conclusions

There is growing awareness that deeper parts of bedrock aquifers in mountain watersheds could be an important part of a watershed's hydrologic system by storing and transmitting larger amounts of water and having a greater influence on stream source than previously indicated. However, deeper parts of mountain aquifers are very difficult to characterize and information on hydraulic conductivity, porosity and flow rates at depth remain scarce and the true importance of deeper groundwater flow across different geologic settings remains highly undertain. This knowledge gap is a major impediment to our ability to predict how surface water flow and its water quality may respond to changes in precipitation, temperature or land use. Deep groundwater flow in a mountain watershed underlain by fractured crystalline rock is increasingly being observed in headwater streams, but it is rarely linked in any robust fashion to the distribution of hydraulic conductivity. Here we present a proof-of-concept for a new and efficient approach for characterizing deeper groundwater flow a in mountain watershed using stream water concentrations of N_2, Ar and SF_6. While shallow and ephemerial interflow produces considerable variability in baseflow age, deeper groundwater flow is found more stable (approx. 12 y) with gas tracer data providing solid evidence of non-trivial grounwater flow to streams that occurs at considerable depth in a mountain watershed underlain by fractured crystalline rock. The implications on the conceptual model of groundwater flow in this mountain watershed is substantial – moving it from strongly topographiclally controlled with groundwater flow paths insensitive to changes in precipitation (and recharge), toward a boarderline recharge controlled groundwater system, such that further drying could have a significant effect on groundwater age contributions to stream water. Work clarifies through a case example the importance of

characterizing the deep bedrock groundwater system in mountain watersheds as a function of where it resides on the R/K spectrum in order to better predict how groundwater and surface water interactions may respond to future changes in climate or land use.

Acknowledgements:

Work was supported by the USGS 104(g) Grant/Cooperative Agreement No. *G16AP00196* and the US Department of Energy Office of Science under contract DE-AC02-05CH11231 as part of Lawrence Berkeley National Laboratory Watershed Function Science Focus Area. Funding from the USGS Mineral Resources Program funded Dr. Manning's time. Additional funding through NSF ROA award #1624073 helped fund Dr. Marchetti. We wish to thank Ward Sanford with the USGS for sharing his baseflow age model template for gas tracer processing and Jerry Casile with the USGS Reston Groundwater Dating Laboratory for his time and expertise on analytical processing of water samples for dissolved gases. We acknowledge the WCU Bartleson-Prather Research Fund for funding WCU undergraduate Manya Ruckhaus who aided in Copper Creek stream and perennial spring sampling. Lastly, we would like to express appreciation to the Rocky Mountain Biological Laboratory for handling Forest Service permitting in the Maroon Bells Wilderness. We appreciate the time and valuable comments from Ward Sanford, Ian Cartwright and two unanimous reviewers. Data and finite difference model approximations of equation 1 are available to the public on the U.S. DOE Environmental Systems Science Data Infrastructure for Virtual Ecosystem (ESS-DIVE).

References Cited

Aeschbach-Hertig, W., Peeters, F., Beyerle, U., Kipfer, R. (2000) 'Paleotemperature reconstruction from noble gases in ground water taking into account equilibration with entrapped air', *Nature*, pp. 1040–1043.

Allen, R. G. *et al.* (2013) 'Sensitivity of Landsat-Scale Energy Balance to Aerodynamic Variability in Mountains and Complex Terrain', *Journal of the American Water Resources Association*, 49(3), pp. 592–604. doi: 10.1111/jawr.12055.

Ameli, A. A. *et al.* (2018) 'Groundwater Subsidy From Headwaters to Their Parent Water

679 Watershed: A Combined Field-Modeling Approach', *Water Resources Research*, 54(7),
680 pp. 5110–5125. doi: 10.1029/2017WR022356.
681 Anderson, B. T. *et al.* (2014) 'Insights into the physical processes controlling correlatinos
682 between snow distribution and terrain properties', *Water Resources Research*, 50, pp.
683 4545–4563. doi: 10.1002/2013WR013714.
684 Badger, A. M., Livneh, B. and Molotch, N. P. (2019) 'On the Role of Spatial Snow Distribution
685 on Alpine Catchment Hydrology', *World Environmental and Water Resources Congress*,
686 pp. 215–225.
687 Bockgard, N., Rodhe, A. and Olsson, K. A. (2004) 'Accuracy of CFC groundwater dating in a
688 crystalline bedrock aquifer: Data from a site in southern Sweden', *Hydrogeology Journal*,
689 12, pp. 171–183.
690 Botter, G., Bertuzzo, E. and Rinaldo, A. (2011) 'Catchment residence and travel time
691 distributions: The master equation', *Geophysical Research Letters*, 38(11), pp. 1–6. doi:
692 10.1029/2011GL047666.
693 Brantley, S. L., Goldhaber, M. B. and Ragnarsdottir, K. V. (2007) 'Crossing disciplines and
694 scales to understand the critical zone', *Elements*, 3(5), pp. 307–314.
695 Brooks, P. D. *et al.* (2015) 'Hydrological partitioning in the critical zone: Recent advances and
696 opportunities for developing transferable understanding of water cycle dynamics', *Water*
697 *Resources Research*, 51, pp. 6973–6987. doi: doi:10.1002/ 2015WR017039.
698 Broxton, P. D. *et al.* (2015) 'Quantifying the effects of vegetation structure on snow
699 accumulation and ablation in mixed-conifer forests', *Ecohydrology*, 8(6), pp. 1073–1094.
700 doi: 10.1002/eco.1565.
701 Busenberg, E. and Plummer, L. N. (2002) 'Dating young water with sulfur hexafluride: natural
702 and anthropogenic sources of sulfur hexafluride', *Water Resources Research*, 36(10), pp.
703 3011–3030. doi: doi:10.1029/2000WR900151.
704 Carroll, R. W. H. *et al.* (2017) 'Evaluating mountain meadow groundwater response to Pinyon-
705 Juniper and temperature in a great basin watershed', *Ecohydrology*, 10(1), pp. 1–18. doi:
706 10.1002/eco.1792.
707 Carroll, R. W. H. *et al.* (2018) 'Factors controlling seasonal groundwater and solute flux from
708 snow-dominated basins', *Hydrological Processes*, 32(14), pp. 2187–2202. doi:
709 10.1002/hyp.13151.

Carroll, R. W. H. *et al.* (2019) 'The Importance of Interflow to Groundwater Recharge in a Snowmelt-Dominated Headwater Basin', *Geophysical Research Letters*, 46(11), pp. 5899–5908. doi: 10.1029/2019GL082447.

Cartwright, I. *et al.* (2018) 'Using geochemistry to understand water sources and transit times in headwater streams of a temperate rainforest', *Applied Geochemistry*, 99, pp. 1–12. doi: https://doi.org/10.1016/j.apgeochem.2018.10.018.

Cartwright, I., Morgenstern, U. and Hofmann, H. (2020) 'Concentration versus streamflow trends of major ions and tritium in headwater streams as indicators of changing water stores', *Hydrological Processes*, 34(2), pp. 485–505. doi: https://doi.org/10.1002/hyp.13600.

Cesano, D., Bagtzoglou, A. C. and Olofsson, B. (2003) 'Quantifying fractured rock hydraulic heterogeneity and groundwater inflow prediction in underground excavations: The heterogeneity index', *Tunnelling and Underground Space Technology*, 18(1), pp. 19–34. doi: 10.1016/S0886-7798(02)00098-6.

Condon, L. E. *et al.* (2020) 'Where Is the Bottom of a Watershed?', *Water Resources Research*, 56(3), pp. 0–3. doi: 10.1029/2019WR026010.

Danesh-Yazdi, M. *et al.* (2018) 'Bridging the gap betwen numerical solutions of travel time distributions and analytical storage selection functions', *Hydrological Processes*, 32(8), pp. 1063–1076. doi: doi:org/10.1002/hyp.11481.

DeBeer, C. M. and Pomeroy, J. W. (2010) 'Simulation of the snowmelt runoff contributing area in a small alpine basin', *Hydrology and Earth System Sciences*, 14, pp. 1205–1219. doi: doi:10.5194/hess-14-1205-2010.

Deems, J. S., Fassnacht, S. R. and Elder, K. J. (2006) 'Fractal distribution of snow depth from LiDAR data', *Journal of Hydrometeorology*, 7, pp. 285–297.

Engdahl, N. B., McCallum, J. L. and Massoudieh, A. (2016) 'Transient age distributions in subsurface hydrologic systems', *Journal of Hydrology*. Elsevier B.V., 543, pp. 88–100. doi: 10.1016/j.jhydrol.2016.04.066.

Fang, Z. *et al.* (2019) 'Streamflow partitioning and transit time distribution in snow-dominated basins as a function of climate', *Journal of Hydrology*. Elsevier, 570(December 2018), pp. 726–738. doi: 10.1016/j.jhydrol.2019.01.029.

Friedrich, R. *et al.* (2013) 'Factors controlling terrigenic SF6 in young groundwater of the

741 Odenwald region (Germany)', *Applied Geochemistry*, 33, pp. 318–329.
742 Frisbee, M. D., Tolley, D. G. and Wilson, J. L. (2016) 'Field estimates of groundwater
743 circulation depths in two mountainous watersheds in the western U.S. and the effect of
744 deep circulation on solute concentrations in streamflow', *Water Resources Research*, 53,
745 pp. 2693–2715. doi: 10.1002/2016WR019553.
746 Frisbee, M. D., Tolley, D. G. and Wilson, J. L. (2017) 'Field estimates of groundwater
747 circulation depths in two mountainous watersheds in the western U.S. and the effect of
748 deep circulation on solute concentrations in streamflow', *Water Resources Research*,
749 53(4), pp. 2693–2715. doi: 10.1002/2016WR019553.
750 Gabrielli, C. P., McDonnell, J. J. and Jarvis, W. T. (2012) 'The role of bedrock groundwater in
751 rainfall-runoff response at hillslope and catchment scales', *Journal of Hydrology*.
752 Elsevier B.V., 450–451, pp. 117–133. doi: 10.1016/j.jhydrol.2012.05.023.
753 Gaskill, D. L. *et al.* (1991) 'Geologic map of the Gothic Quadrangle, Gunnison County,
754 Colorado'.
755 Gleeson, T. *et al.* (2018) 'The suitability of using dissolved gases to determine groundwater
756 discharge to high gradient streams', *Journal of Hydrology*. Elsevier B.V., 557, pp. 561–
757 572. doi: 10.1016/j.jhydrol.2017.12.022.
758 Gleeson, T. and Manning, A. H. (2008) 'Regional groundwater flow in mountainous terrain:
759 Three-dimensional simulations of topographic and hydrogeologic controls', *Water*
760 *Resources Research*, 44(10), pp. 1–16. doi: 10.1029/2008WR006848.
761 Hale, V. C. and McDonnell, J. J. (2016) 'Effect of bedrock permeability on stream base flow
762 mean transit time scaling relations: 1. A multiscale catchment intercomparison', *Water*
763 *Resources Research*, 52(2), pp. 1358–1374. doi: 10.1002/2014WR016124.
764 Harbaugh, A. W. (2005) 'MODFLOW-2005, the U.S. Geological Survey Modular Groundwater
765 Model – The Ground-Water Flow Process', *U.S. Geological Survey Technical Methods,*
766 *Book 6*, p. Ch. A16.
767 Harman, C. J. (2015) 'Time-variable transit time distributions and transport: Theory and
768 application to storage-dependent transport of chloride in awatershed', *Water Resources*
769 *Research*, 51(1), pp. 1–30. doi: 10.1002/2014WR015707.Received.
770 Harpold, A. *et al.* (2012) 'Changes in snowpack accumulation and ablation in the intermountain
771 west', *Water Resources Research*, 48(11). doi: 10.1029/2012WR011949.

772 Hay, L. E., Markstrom, S. L. and Ward-Garrison, C. D. (2011) 'Watershed-scale response to
773 climate change through the 21st century for selected basins across the United States',
774 *Earth Interactions*, 15, pp. 1–37.
775 Heidbüchel, I. *et al.* (2012) 'The master transit time distribution of variable flow systems', *Water*
776 *Resources Research*, 48(6), pp. 1–19. doi: 10.1029/2011WR011293.
777 Howcroft, W., Cartwright, I. and Morgenstern, U. (2018) 'Mean transit times in headwater
778 catchments: Insights from the Otway Ranges, Australia', *Hydrology and Earth System*
779 *Sciences*, 22(1), pp. 635–653. doi: 10.5194/hess-22-635-2018.
780 Hrachowitz, M. *et al.* (2013) 'What can flux tracking teach us about water age distribution
781 patterns and their temporal dynamics?', *Hydrology and Earth System Sciences*, 17(2), pp.
782 533–564. doi: 10.5194/hess-17-533-2013.
783 Hubbard, S. S. *et al.* (2018) 'The East River, Colorado, watershed: A mountainous community
784 testbed for improving predictive understanding of multiscale hydrological–
785 biogeochemical dynamics', *Vadose Zone Journal*, 17(1). doi: 10.2136/vzj2018.03.0061.
786 Huntington, J. L. and Niswonger, R. G. (2012) 'Role of surface-water and groundwater
787 interactions on projected summertime streamflow in snow-dominated regions: an
788 integrated modeling approach', *Water Resources Research*, 48. doi:
789 10.1029/2012WR012319.
790 IPCC (2019) 'IPCC Special Report on the Ocean and Cryosphere in a Changing Climate [H.-O.
791 Pörtner Roberts, D.C. Masson-Delmotte, V. Zhai, P. Tignor, M. Poloczanska, E.
792 Mintenbeck, K. Nicolai, M. Okem, A. Petzold, J. B. Rama, N. Weyer (eds.)]', *In press*,
793 (September). doi: https://www.ipcc.ch/report/srocc/.
794 Jasechko, S. *et al.* (2016) 'Substantial proportion of global streamflow less than three
795 months old', *Nature Geoscience*, 9(2), pp. 126–129. doi: 10.1038/ngeo2636.
796 Katsura, S. *et al.* (2009) 'Hydraulic properties of variously weathered granitic bedrock in
797 headwater catchments', *Vadose Zone Journal*, 8(3), p. 557. doi:
798 doi:10.2136/vzj2008.0142.
799 Kirchner, J. W. (2009) 'Catchments as simple dynamical systems: catchment characterization,
800 rainfall-runoff modeling, and doing hydrology backward', *Water Resources Research*,
801 45. doi: DOI:10.1029/2008WR006912.
802 Kolbe, T. *et al.* (2016) 'Coupling 3D groundwater modeling with CFC-based age dating to

803 classify local groundwater circulation in an unconfined crystalline aquifer', *Journal of*
804 *Hydrology*. Elsevier B.V., 543, pp. 31–46. doi: 10.1016/j.jhydrol.2016.05.020.
805 LANDFIRE (2015) *Existing vegetation type and cover layers, U.S. Department of the Interior,*
806 *Geological Survey*. Available at: http://landfire.cr.usgs.gov/viewer/(accessed May 2017).
807 Mahlknecht, J. *et al.* (2017) 'Understanding the dynamics and contamination of an urban aquifer
808 system using groundwater age (14C, 3H, CFCs) and chemistry', *Hydrological Processes*,
809 31(13), pp. 2365–2380. doi: 10.1002/hyp.11182.
810 Manning, A. H. (2009) 'Ground-water temperature, noble gas, and carbon isotope data from the
811 Española Basin, New Mexico', *U.S. Geological Survey Scientific Investigations Report*,
812 2008–5200, p. 69 p.
813 Manning, A. H. *et al.* (2012) 'Evolution of groundwater age in a mountain watershed over a
814 period of thirteen years', *Journal of Hydrology*. Elsevier B.V., 460–461, pp. 13–28. doi:
815 10.1016/j.jhydrol.2012.06.030.
816 Manning, A. H. *et al.* (2013) 'Links between climate change, water-table depth, and water
817 chemistry in a mineralized mountain watershed', *Applied Geochemistry*, 37(October
818 2016), pp. 64–78. doi: 10.1016/j.apgeochem.2013.07.002.
819 Manning, A. H. *et al.* (2019) 'Using stream-side groundwater discharge for geochemical
820 exploration in mountainous terrain', *Journal of Geochemical Exploration*, 309. doi:
821 doi.org/10.1016/j.gexplo.2019.106415.
822 Markovich, K. H. *et al.* (2019) 'Mountain-block Recharge: A Review of Current Understanding'.
823 doi: 10.1029/2019WR025676.
824 Markstrom, S. L. *et al.* (2008) 'GSFLOW – Coupled Ground-Water and Surface-Water Flow
825 Model Based on the Integration of the Precipitation-Runoff Modeling System (PRMS)
826 and the Modular Ground-Water Flow Model (MODFLOW-2005)':, *U.S. Geological*
827 *Survey Techniques and Methods*, 6-D1, p. 240.
828 Markstrom, S. L. *et al.* (2015) 'PRMS-IV, the precipitation-runoff modeling system, version 4',
829 *U.S. Geological Survey Techniques and Methods, book 6, chap. B7*, p. 158. doi:
830 http://dx.doi.org/10.3133/tm6B7.
831 Maxwell, R. M. *et al.* (2016) 'The imprint of water and geology on residence times in
832 groundwater', *Geophysical Research Letters*, 43, pp. 701–708. doi:
833 doi:10.1002/2015GL066916.

McGuire, K. J. *et al.* (2005) 'The role of topography on catchment-scale water residence time', *Water Resources Research*, 41(5). doi: 10.1029/2004WR003657.

McGuire, K. J. and McDonnell, J. J. (2006) 'A review and evaluation of catchment transit time modeling', *Journal of Hydrology*, 330(3–4), pp. 543–563. doi: 10.1016/j.jhydrol.2006.04.020.

Meixner, T. *et al.* (2016) 'Implications of projected climate change for groundwater recharge in the western United States', *Journal of Hydrology*. Elsevier B.V., 534(January), pp. 124–138. doi: 10.1016/j.jhydrol.2015.12.027.

Meyer, J. L. *et al.* (2007) 'The contribution of headwater streams to biodiversity in river networks', *Journal of the American Water Resources Association*, 43(1), pp. 86–103. doi: 10.1111/j.1752-1688.2007.00008.x.

Miller, M. P. *et al.* (2016) 'The importance of base flow in sustaining surface water flow in the Upper Colorado River Basin', *Water Resources Research*, 52(5), pp. 3547–3562. doi: 10.1002/2015WR017963.Received.

Missik, J. E. C. *et al.* (2019) 'Groundwater-River Water Exchange Enhances Growing Season Evapotranspiration and Carbon Uptake in a Semiarid Riparian Ecosystem', *Journal of Geophysical Research: Biogeosciences*, 124(1), pp. 99–114. doi: 10.1029/2018JG004666.

Musselman, K. N., Molotch, N. P. and Brooks, P. D. (2008) 'Effects of vegetation on snow accumulation and ablation in a mid-latitude sub-alpine forest', *Hydrological Processes*, 22(15), pp. 2767–2776. doi: 10.1002/hyp.7050.

Niswonger, R. G., Panday, S. and Ibaraki, M. (2011) 'MODFLOW-NWT, A Newton Formulation for MODFLOW-2005', *U.S. Geological Survey Groundwater Resources Program, Techniques and Methods*, 6-A37, p. 44.

NRCS (1991) *Web Soil Survey, United States Department of Agriculture*. Available at: http://websoilsurvey.nrcs.usda.gov/accessed March 2016.

Onda, Y. *et al.* (2006) 'Runoff generation mechanisms in high-relief mountainous watersheds with different underlying geology', *Journal of Hydrology*, 331, pp. 659–673. doi: https://doi.org/10.1016/j.jhydrol.2006.06.009.

Painter, T. H. *et al.* (2016) 'The Airborne Snow Observatory: Fusion of scanning lidar, imaging spectrometer, and physically-based modeling for mapping snow water equivalent and

865 snow albedo', *Remote Sensing of Environment*. Elsevier Inc., 184, pp. 139–152. doi:
866 10.1016/j.rse.2016.06.018.
867 Perdrial, J. *et al.* (2018) 'A net ecosystem carbon budget for snow dominated forested headwater
868 catchments: linking water and carbon fluxes to critical zone carbon storage',
869 *Biogeochemistry*, 138(3), pp. 225–243. doi: 10.1007/s10533-018-0440-3.
870 Plummer, L. N. *et al.* (2001) 'Groundwater residence times in Shenandoah National Park, Blue
871 Ridge Mountains, Virginia, USA: a multi-tracer approach', *Chemical Geology*, 179, pp.
872 93–111.
873 Pollock, D. W. (2016) 'User guide for MODPATH Version 7 -- a particle-tracking model for
874 MODFLOW', *U.S. Geological Survey Open-File Report*, 2016–1086, p. 35 p. doi:
875 10.3133/ofr20161086.
876 Rukundo, E. and Doğan, A. (2019) 'Dominant influencing factors of groundwater recharge
877 spatial patterns in Ergene river catchment, Turkey', *Water (Switzerland)*, 11(4). doi:
878 10.3390/w11040653.
879 Rumsey, C. A. *et al.* (2015) 'Regional Studies Regional scale estimates of baseflow and factors
880 influencing baseflow in the Upper Colorado River Basin', *Journal of Hydrology*. Elsevier
881 B.V., 4, pp. 91–107.
882 Sanford, W. E., Casile, G. and Haase, K. B. (2015) 'Dating base flow in streams using dissolved
883 gases and diurnal temperature changes', *Water Resources Research*, pp. 1–14. doi:
884 10.1002/2014WR016796.
885 Smith, A. A., Tetzlaff, D. and Soulsby, C. (2018) 'Using StorAge Selection functions to quantify
886 ecohydrological controls on the time-variant age of evapotranspiration, soil water, and
887 recharge', *Hydrology and Earth System Sciences Discussions*, (February), pp. 1–25. doi:
888 10.5194/hess-2018-57.
889 Solomon, D. K., Cook, P. G. and Sanford, W. E. (1998) *Dissolved gases in subsurface
890 hydrology*, *Isotope Tracers in Catchment Hydrology*. Edited by C. Kendall and J.
891 McDonnell. Amsterdam: Elsevier.
892 Stute, M. and Schlosser, P. (2000) 'Atmospheric noble gases', in Cook, P. G. and Herczeg, A. L.
893 (eds) *Environmental Tracers in Subsurface Hydrology*. New York: Springer, pp. 349–
894 377.
895 Tetzlaff, D. *et al.* (2009) 'How does landscape sturcture influence catchment scale transit time

across different geomorphic provinces?', *Hydrological Processes*, 23, pp. 945–953.

Toth, J. (1963) 'A theoretical analysis of groundwater flow in small drainage basins', *Journal of Geophysical Research*, 68, pp. 4795–4812. doi: doi:10.1029/JZ068i008p02354.

Tullborg, E.-L. and Larson, S. A. (2006) 'Porosity in crystalline rocks – A matter of scale', *Engineering Geology*, 84(1–2), pp. 75–83. doi: https://doi.org/10.1016/j.enggeo.2005.12.001.

USGS (2017) *U.S. Geological Survey Groundwater Age Dating Laboratory*, *U.S. Geological Survey, Reston, VA*. Available at: http://water.usgs.gov/lab/ (Accessed: 23 March 2017).

Van Der Velde, Y. *et al.* (2012) 'Quantifying catchment-scale mixing and its effect on time-varying travel time distributions', *Water Resources Research*, 48(6), pp. 1–13. doi: 10.1029/2011WR011310.

Visser, A. *et al.* (2019) 'Cosmogenic Isotopes Unravel the Hydrochronology and Water Storage Dynamics of the Southern Sierra Critical Zone', *Water Resources Research*, pp. 1429–1450. doi: 10.1029/2018WR023665.

Viviroli, D. and Weingartner, R. (2008) 'Water Towers- A Global View of the Hydrological Imporants of Mountains.', *Mountains: Sources of Water, Sources of Knowledge*, pp. 15–20.

Wang, K. and Dickinson, R. (2012) 'a Review of Global Terrestrial Evapotranspiration : Observation, Modeling, Climatology, and Climate Variability', *Reviews of Geophysics*, 50(2011), pp. 1–54. doi: 10.1029/2011RG000373.1.INTRODUCTION.

Welch, L. A. and Allen, D. M. (2014) 'Caractéristiques de la conductivité hydraulique en région de montagne et implications pour la conceptualisation des écoulements souterraines dans la roche en place', *Hydrogeology Journal*, 22(5), pp. 1003–1026. doi: 10.1007/s10040-014-1121-5.

Winnick, M. J. *et al.* (2017) 'Snowmelt controls on concentration-discharge relationships and the balance of oxidative and acid-base weathering fluxes in an alpine catchment, East River, Colorado', *Water Resources Research*, 53. doi: 10.1002/2016WR019724.

Winter, T. C., Rosenberry, D. O. and LaBaugh, J. W. (2001) 'The concept of hydrologic landscapes', *Journal of American Water Resources Association*, 37, pp. 335–349. doi: doi:10.111/j.1752-1688.2001.tb00973.x.

927 Table 1: Geologic units in Copper Creek and model specified parameters.

Symbol	Epoch	Name	Description (modified Gaskill et al., 1991)	Surface[a] K (m/s)	VKA[b]	Surface[a] Porosity	Deep[c] Porosity
Qal	Holocene	Surface Deposits	alluvium, fans, debris flow, landslide, talus, rock glaciers	$1.2x10^{-5}$ $1.1x10^{-4}$	1	0.2	0.1
Tg	Oligocene	Granodiorite	White Rock Pluton - quartz diorite to quartz manzonite	$4.6x10^{-7}$	3	0.025	0.0125
Sill	Oligocene	Granodiorite	Quartz diorite to quartz manzonite	$4.6x10^{-7}$	3	0.025	0.0125
Km1	Upper Cretaceous	Main Body Mancos Shale	mostly silty to sandy marine shale	$1.2x10^{-6}$	3	0.1	0.05
Km2	Upper Cretaceous	Lower Member Mancos Shale	interbedded silty and sandy, calcareous marine shale, siltstone	$1.2x10^{-6}$	3	0.1	0.05
Kd	Upper Cretaceous	Dakota Sandstone	quartzitic sandstone grading upward to carbonaceous shale, sandstone, siltstone to fine granded quartite	$5.8x10^{-6}$	3	0.1	0.05
JmJe	Upper/Middle Jurassic	Morrison Fm & Entrada Sandstone	Jm: claystone, siltstone, and shale (65%) interlensed with cherty sandstone (30%). Je:thick bedded, cross-laminated quartz-arenite, or quartzite	$1.2x10^{-6}$	3	0.1	0.05
PPm	Lower Permian/Upper-Middle Pensnsylvanian	Maroon Fm	siltstone and sandstone interbedded with conglomerate, mudstone and limestone	$5.8x10^{-6}$	3	0.1	0.05
Pg	Middle Pennsylvanian	Gothic Fm	Interbedded sandstone, limestone, siltstone, shale and conglomerate. Metamorphosed along igneous contact	$1.2x10^{-6}$	3	0.1	0.05

[a]surface applies to model layer 1 and 2 (≤18m). K assumed to decline exponentially with depth

[b]ratio of vertical to horizontal hydraulic conductivity (anisotropy)

[c]deep applies to model layers 3-12 (18 - 400 m)

928

929 Table 2. Selected model solutions for stream dissolved gas concentrations.

Modeled Gases	Estimated Parameters									χ^2 Sum	p = 0.1 χ^2 Sum	Acceptable Fit?
	EA (cm^3STP/g)	C_{xn} mg/L	T_r (°C)	τ_w (h)	τ_{gnar} (h)	τ_{gsf6} (h)	τ_{g113} (h)	SF_6 C_{gw} (fmol/L)	CFC-113 C_{gw} (pmol/L)	(-)	(-)	
N_2, Ar	0.000	0.0	10.0	10.7	0.07	--	--	--	--	12.6	24.8	Yes
N_2, Ar	0.010	0.0	0.0	14.1	0.08	--	--	--	--	10.6	24.8	Yes
SF_6, CFC-113	--	--	--	0.83	--	0.06	0.08	1.32	0.228	19.1	27.2	Yes
SF_6, CFC-113	--	--	--	0.50	--	0.06	0.07	1.89	0.267	21.9	27.2	Yes
SF_6, CFC-113	--	--	--	1.50	--	0.07	0.14	0.58	0.218	20.7	27.2	Yes
SF_6, CFC-113	--	--	--	4.00	--	0.31	0.14	1.35	0.000	24.9	27.2	Yes
SF_6	--	--	--	0.61	--	0.25	--	2.66	--	100.4	14.7	No
SF_6	--	--	--	0.91	--	0.37	--	2.60	--	71.8	14.7	No
SF_6	--	--	--	1.31	--	0.46	--	2.50	--	42.1	14.7	No
SF_6	--	--	--	1.69	--	0.48	--	2.40	--	26.5	14.7	No
SF_6	--	--	--	2.07	--	0.49	--	2.30	--	17.9	14.7	No
SF_6	--	--	--	2.44	--	0.48	--	2.20	--	12.9	14.7	Yes
SF_6	--	--	--	2.80	--	0.47	--	2.10	--	9.8	14.7	Yes
SF_6	--	--	--	3.15	--	0.46	--	2.00	--	7.8	14.7	Yes
SF_6	--	--	--	4.84	--	0.43	--	1.50	--	4.0	14.7	Yes
SF_6	--	--	--	6.47	--	0.41	--	1.00	--	3.2	14.7	Yes
SF_6	--	--	--	8.08	--	0.40	--	0.50	--	3.0	14.7	Yes
SF_6	--	--	--	9.68	--	0.39	--	0.00	--	2.9	14.7	Yes

See text for definitions of model parameters; cm^3STP/g = cubic centimeters at standard temperature and pressure per gram of water; underlined parameter values were specified not estimated; -- = not estimated or computed; NA = not applicable

930

931

Table 3. Simulated median ages for groundwater and baseflow in Copper Creek for historic climate conditions.

Water Year	late Aug. Infterflow (fraction)	Median Age (Years)		Climate Condition
		Groundwater Only	Baseflow*	
1995	0.50	11.57	3.30	Wettest year on record, largest snowpack and latest snowmelt
1998	0.19	11.66	7.80	Median Water Year
2002	0.03	11.51	11.41	Multiple-year drought 2000-2002
2012	0.20	11.89	7.62	Single large drought after wet year, good monsoon
2017	0.22	12.17	7.48	Wet year, gas tracer experiment
2018	0.01	12.11	11.91	Single large drought after wet year, poor monsoon

*includes interflow

List of Figures

Figure 1. (a) The East River with Copper Creek delineated. Inset shows location of the site in the context of the western United States and the Upper Colorado River Basin. (b) Geologic cross section A-A' modified from (Gaskill *et al.*, 1991) with geologic units described in Table 1.

Figure 2. Sampling location CC03 (a) Sum χ^2 between predicted and observed stream water concatenations as a function of contribution groundwater SF_6 concentration. GSFLOW related metrics indicated. (b) SF_6 observed water column concentrations with best fit predicted water column concentrations using baseflow age distributions from original GSFLOW and recalibrated GSFLOW simulation.

Figure 3. Copper Creek simulated stream conditions (at the basin outlet) for the recalibrated GSFLOW model to illustrate interannual variability in stream water source across a range of historical climate conditions; (a) streamflow, (b) the fraction of streamflow that is interflow.

Figure 4. (a) GSFLOW recharge weighted baseflow age cumulative distribution (F(t)) for late August 2017 at the sampling site CC03 and best fit Weibull distributions to calculate stream water SF_6 concentrations shown in Figure 3. Age range of springs based on gas data collected in October 2017 provided. Weibull parameters (refer to equation 3) for the original GSFLOW model k = 0.28, n =0.44; and for the recalibrated GSFLOW model k = 0.08, n = 0.66. (b) GSFLOW recharge weighted maximum depth of groundwater flow through alluvial and bedrock units (F(depth)) at the watershed outlet. Symbols placed at average depth of model layers 1 to 12.

Figure 5. Groundwater flow path ages through the saturated subsurface for (a) the original GSFLOW model and (b) the recalibrated GSFLOW model. The sampling location for the gas tracer experiment (CC03) and the watershed outlet identified.

Figure 6: Sensitivity of groundwater median age to drying, warming and forest removal scenarios with respect to (a) precipitation; and (b) basin-wide net recharge, defined as soil seepage below the rooting zone + stream losses to the groundwater system – groundwater ET.

966 The historic median water year precipitation = 1.28 m/y and corresponding quasi-steady state net
967 recharge (0.22 m/y) separate recharge and topographically controlled groundwater flow paths.
968
969 Figure 7. Conceptual model of groundwater flow: (a) topographically controlled flow with a high
970 recharge to hydraulic conductivity ratio (R/K). Baseflow median age insensitive to surface
971 dynamics controlling net recharge. (b) Recharge-controlled groundwater flow with a low R/K.
972 Baseflow median age is sensitive to surface processes dictating recharge. ET_{gw} = groundwater
973 ET.

Figure 1.

(a)

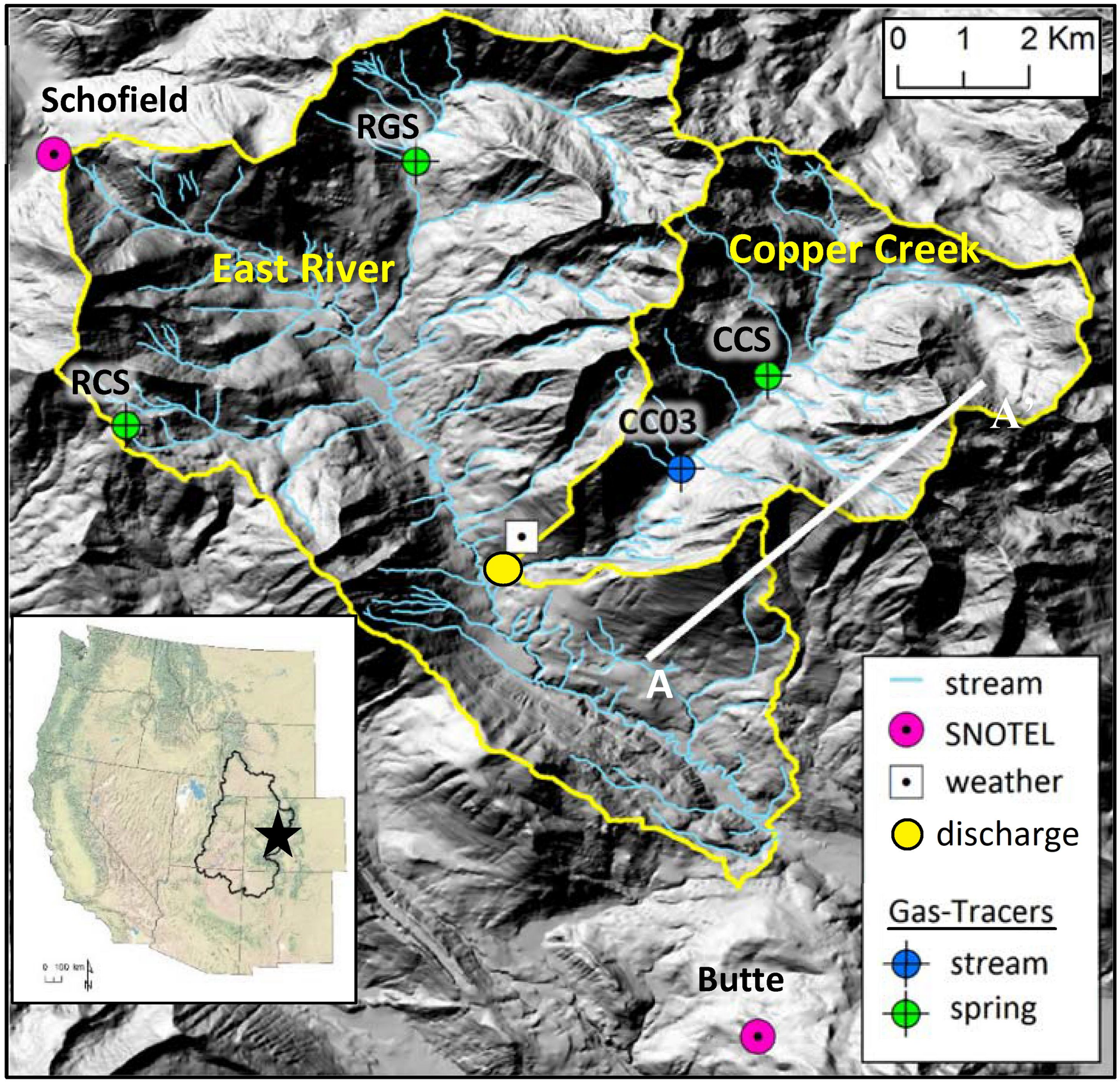
0 1 2 Km
Schofield
RGS
East River
Copper Creek
CCS
RCS
CC03
A'
A
stream
SNOTEL
weather
discharge
Gas-Tracers
stream
spring
Butte
0 100 km
N

(b)

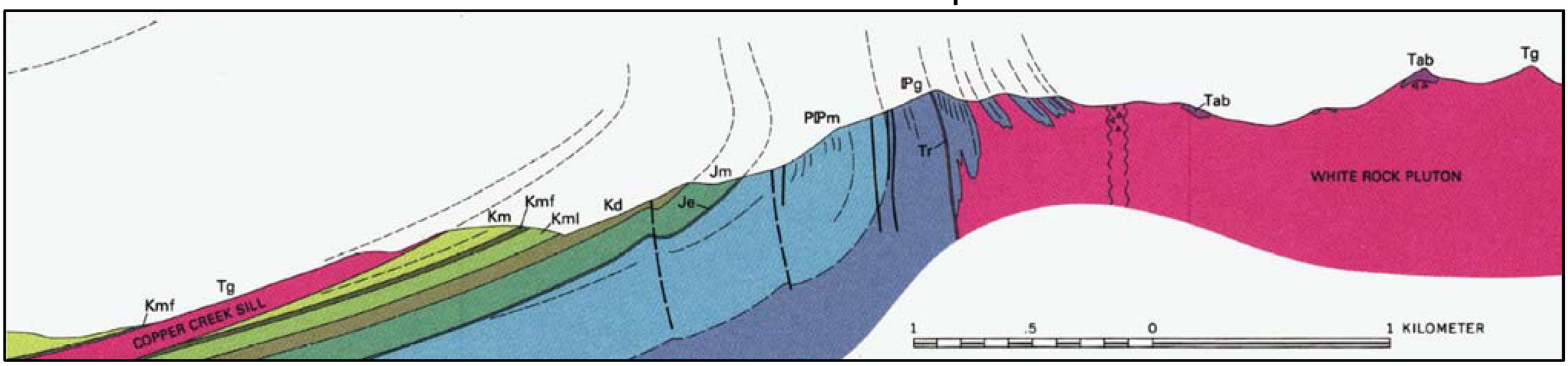
Lower Copper Creek
Upper Copper Creek
Tg
Tab
Tab
Pg
PPm
Tr
Jm
Je
Kd
Km
Kmf
Kml
Kmf
Tg
COPPER CREEK SILL
WHITE ROCK PLUTON
1 .5 0 1 KILOMETER

A A'

Figure 2.

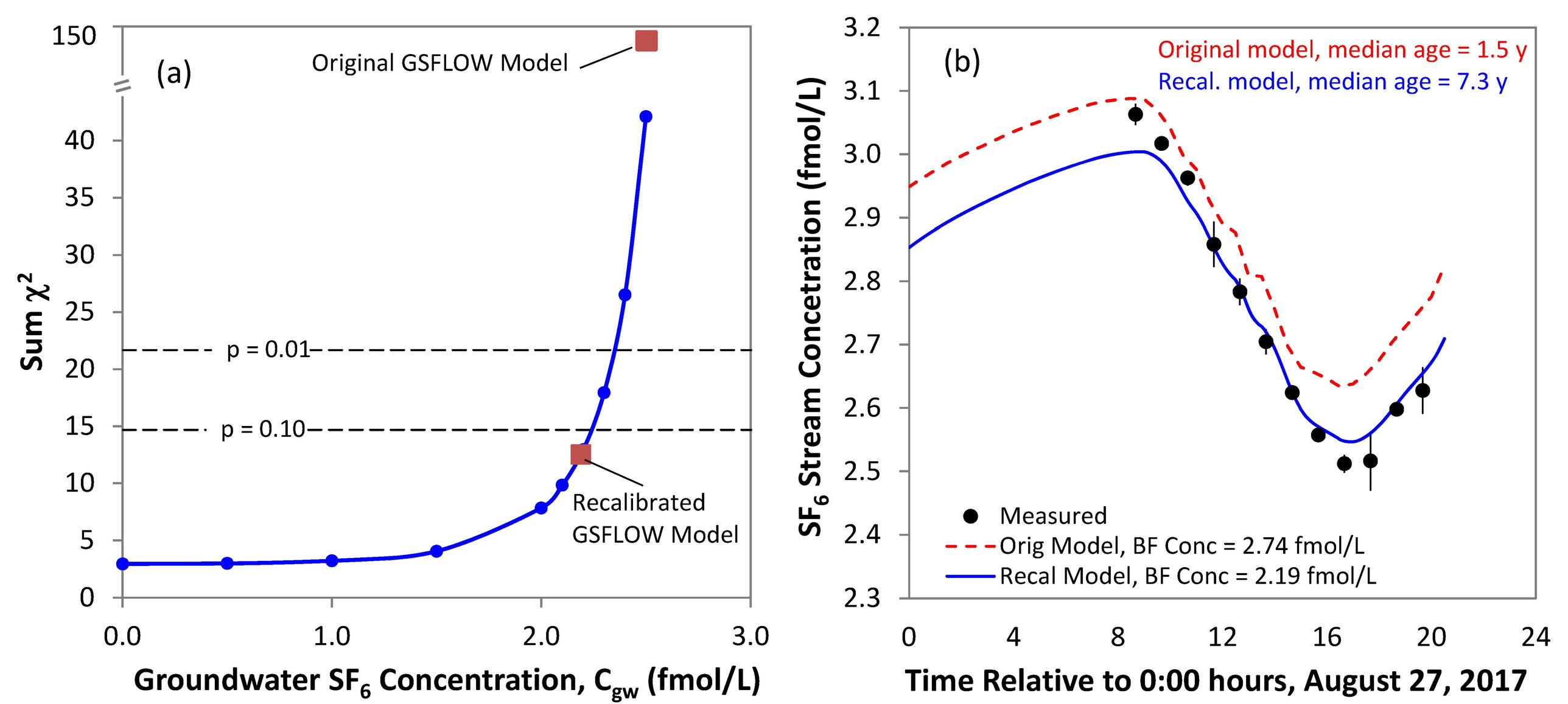
(a)
Original GSFLOW Model
p = 0.01
p = 0.10
Recalibrated
GSFLOW Model
Sum χ²
Groundwater SF6 Concentration, Cgw (fmol/L)
(b)
Original model, median age = 1.5 y
Recal. model, median age = 7.3 y
Measured
Orig Model, BF Conc = 2.74 fmol/L
Recal Model, BF Conc = 2.19 fmol/L
SF6 Stream Concetration (fmol/L)
Time Relative to 0:00 hours, August 27, 2017

Figure 3.

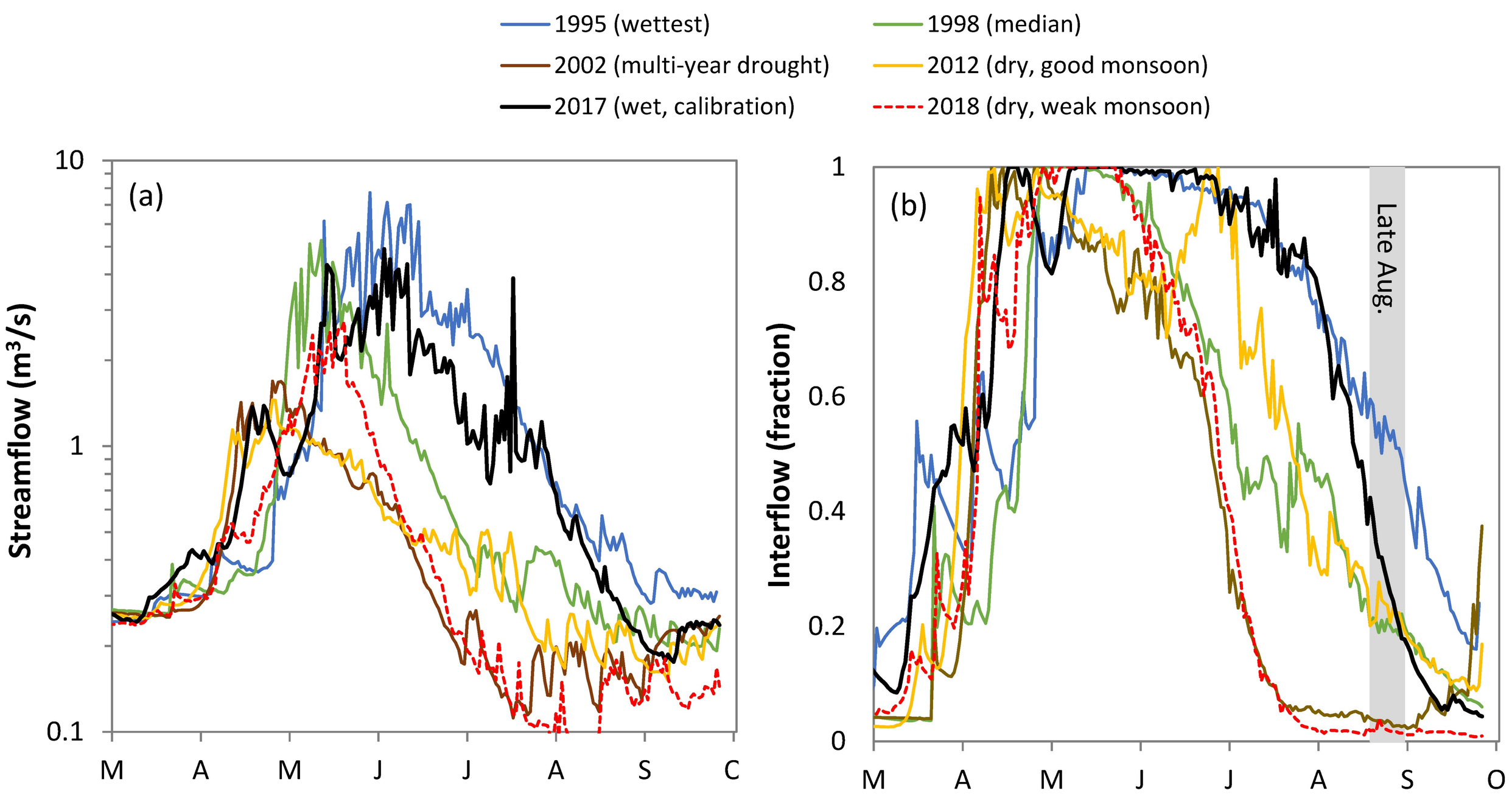
1995 (wettest)
1998 (median)
2002 (multi-year drought)
2012 (dry, good monsoon)
2017 (wet, calibration)
2018 (dry, weak monsoon)
(a)
Streamflow (m³/s)
10
1
0.1
M
A
M
J
J
A
S
O
(b)
Interflow (fraction)
1
0.8
0.6
0.4
0.2
0
Late Aug.

Figure 4.

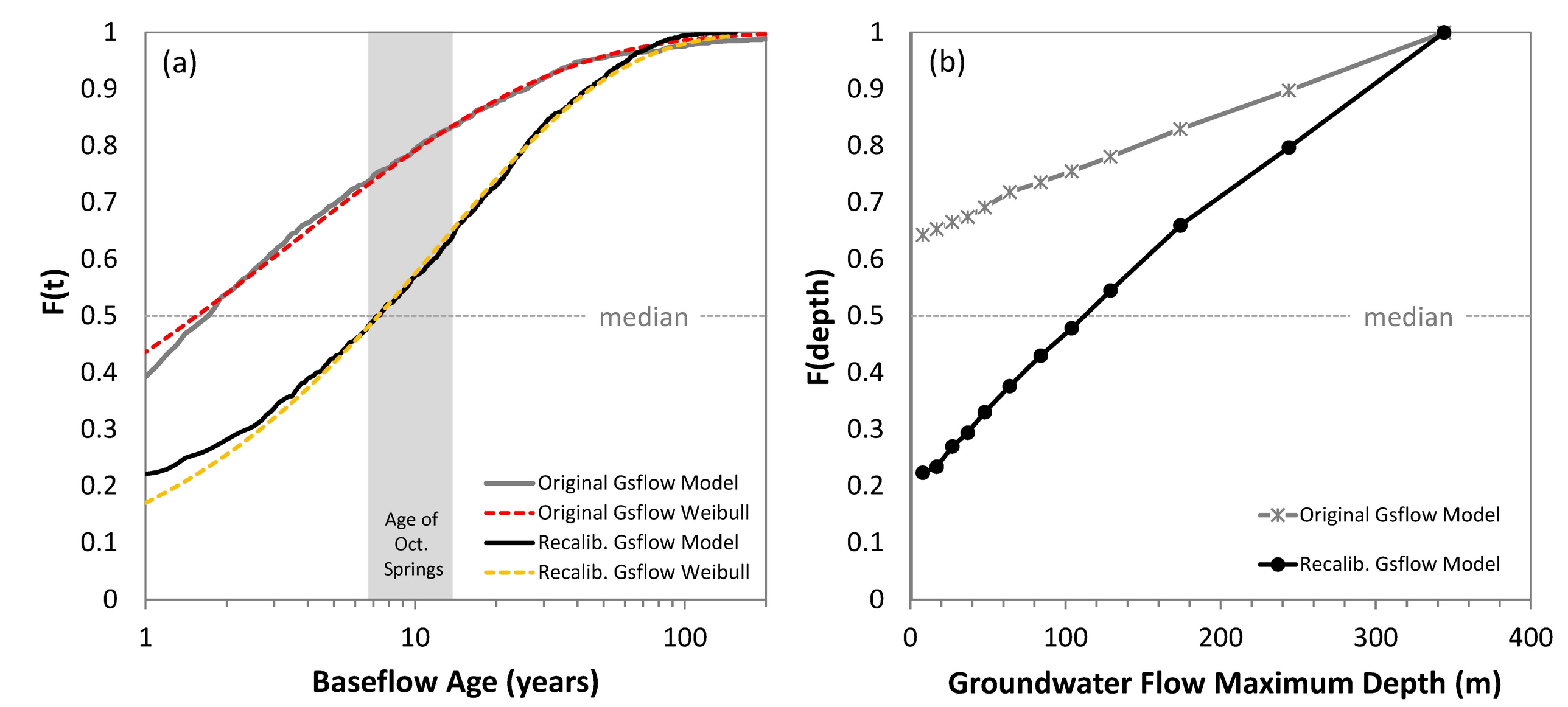
(a)
F(t)
1
0.9
0.8
0.7
0.6
0.5
0.4
0.3
0.2
0.1
0
median
Age of Oct. Springs
Original Gsflow Model
Original Gsflow Weibull
Recalib. Gsflow Model
Recalib. Gsflow Weibull
1
10
100
Baseflow Age (years)
(b)
F(depth)
median
Original Gsflow Model
Recalib. Gsflow Model
0
100
200
300
400
Groundwater Flow Maximum Depth (m)

Figure 5.

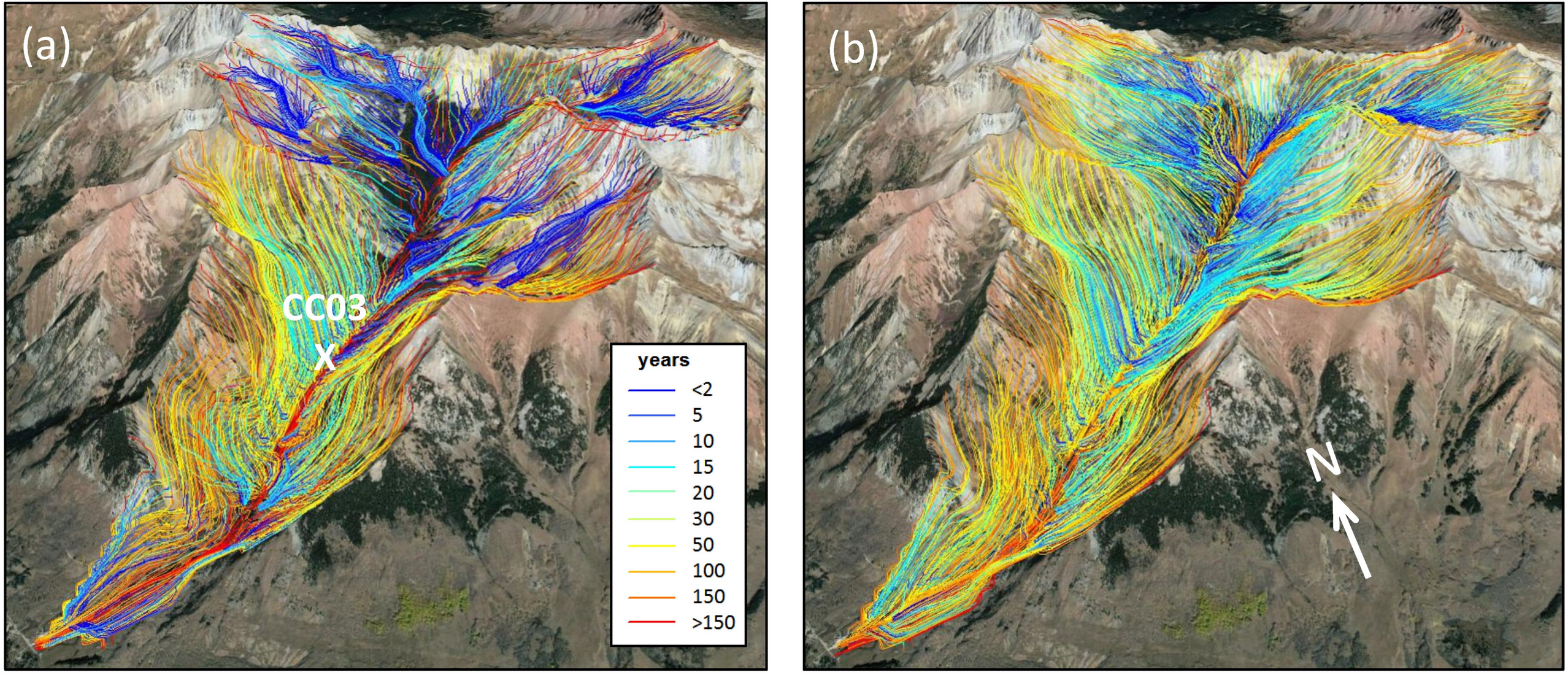
(a)
CC03
years
<2
5
10
15
20
30
50
100
150
>150
(b)
N

Figure 6.

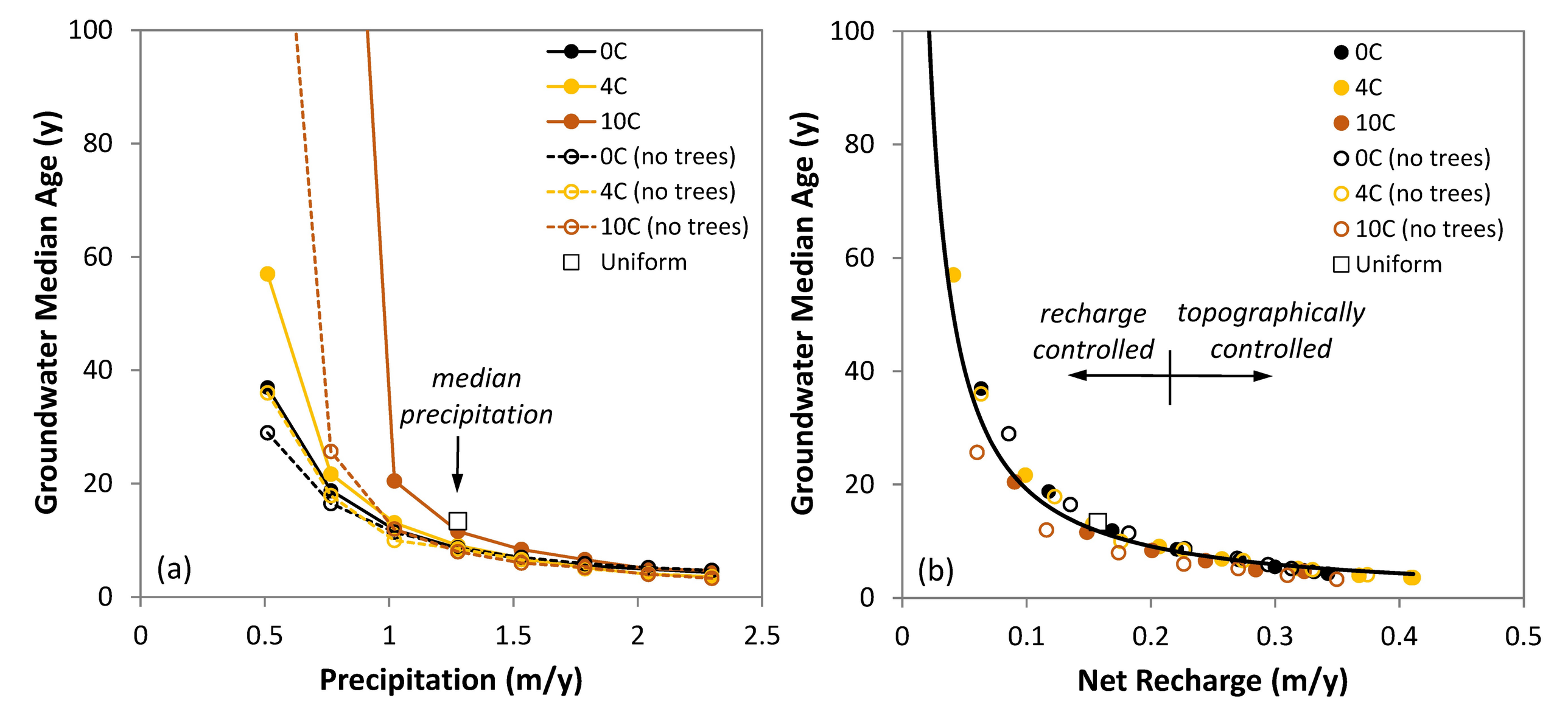
Groundwater Median Age (y)
Precipitation (m/y)
0C
4C
10C
0C (no trees)
4C (no trees)
10C (no trees)
Uniform
median
precipitation
(a)
Groundwater Median Age (y)
Net Recharge (m/y)
recharge
controlled
topographically
controlled
(b)

Figure 7.

Redistribution
Water Table
Snow
Recharge
Perennial Stream
Fractured Bedrock Low K
Groundwater
Young
Intermediate
Old
ET_{gw}
Stream
Alluvium High K
CDF
1
0.8
0.6
0.4
0.2
0
1
10
100
Age (year)
(a)
Alpine
Subalpine
Montane
Riparian
EESA19-064

Redistribution
Snow
Water Table
Recharge
Ephemeral Stream
Fractured Bedrock Low K
Groundwater
Young
Intermediate
Old
ET_{gw}
Stream
Alluvium High K
CDF
1
0.8
0.6
0.4
0.2
0
1
10
100
Age (year)
(b)
Alpine
Subalpine
Montane
Riparian
EESA19-065